Modeling the Frozen-In Anticyclone in the 2005 Arctic Summer Stratosphere

D. R. Allen[1], A. R. Douglass[2], G. L. Manney[3,4], S. E. Strahan[5], J. C. Krosschell[6], J. Trueblood[6]

[1]{Naval Research Laboratory, Washington, DC}

[2]{NASA Goddard Space Flight Center, Greenbelt, MD}

[3]{Jet Propulsion Laboratory, California Institute of Technology, Pasadena, CA}

[4]{Department of Physics, New Mexico Institute of Mining and Technology, Socorro, NM}

[5]{Goddard Earth Science and Technology Center, University of Maryland Baltimore County, Baltimore, MD}

[6]{Dordt College, Sioux Center, IA}

Correspondence to: D. R. Allen (Douglas.Allen@nrl.navy.mil)

Abstract

Immediately following the breakup of the 2005 Arctic spring stratospheric vortex, a tropical air mass, characterized by low potential vorticity (PV) and high nitrous oxide (N_2O), was advected poleward and became trapped in the easterly summer polar vortex. This feature, known as a "Frozen-In Anticyclone (FrIAC)", was observed in Earth Observing System (EOS) Aura Microwave Limb Sounder (MLS) data to span the potential temperature range from ~580 to 1100 K (~25 to 40 km altitude) and to persist from late March to late August 2005. This study compares MLS N_2O observations with simulations from the Global Modeling Initiative (GMI) chemistry and transport model, the GEOS-5/MERRA Replay model, and the Van Leer Icosahedral Triangular Advection (VITA) isentropic transport model to elucidate the processes involved in the lifecycle of the FrIAC, which is here divided into three distinct phases. During the "spin-up phase" (March to early April), strong poleward flow resulted in a tight isolated anticyclonic vortex at ~70–90°N, marked with elevated N_2O. GMI, Replay, and VITA all reliably simulated the spin-up of the FrIAC, although the GMI

1   and Replay peak N_2O values were too low. The FrIAC became trapped in the developing

2   summer easterly flow and circulated around the polar region during the "anticyclonic phase"

3   (early April to the end of May). During this phase, the FrIAC crossed directly over the pole

4   between the 7th and 14th of April. The VITA and Replay simulations transported the N_2O

5   anomaly intact during this crossing, in agreement with MLS, but unrealistic dispersion of the

6   anomaly occurred in the GMI simulation due to excessive numerical mixing of the polar cap.

7   The vortex associated with the FrIAC was apparently resistant to the weak vertical shear

8   during the anticyclonic phase, and it thereby protected the embedded N_2O anomaly from

9   stretching. The vortex decayed in late May due to diabatic processes, leaving the N_2O

10 anomaly exposed to horizontal and vertical wind shears during the "shearing phase" (June to

11 August). The observed lifetime of the FrIAC during this phase is consistent with time-scales

12 calculated from the ambient horizontal and vertical wind shear. Replay maintained the

13 horizontal structure of the N_2O anomaly similar to MLS well into August. The VITA

14 simulation also captured the horizontal structure of the FrIAC during this phase, but VITA

15 eventually developed fine-scale N_2O structure not observed in MLS data.

16 **1 Introduction**

17 The winter-to-summer transition in the Arctic stratosphere has been examined in numerous

18 observational and modeling studies, and a good general understanding of the processes

19 governing this transition has developed. A consistent finding is that as the winter polar vortex

20 breaks up in the final warming, complicated remnants of winter polar vortex air are

21 intermingled with extra-vortex air. These two distinct air masses may remain relatively

22 unmixed in the stratosphere for several months. The winter polar vortex remnants are marked

23 by anomalies in dynamical fields and long-lived chemical tracers. The signature in the

24 dynamical fields (e.g., potential vorticity or potential temperature) tends to decay on a

25 timescale of 1–2 months due to diabatic processes (Hess, 1990, 1991), whereas anomalies in

26 chemical tracers (e.g., low nitrous oxide) can last much longer, persisting even until late

27 August (Orsolini, 2001). These features are said to be "frozen-in" to the summer easterly jet,

28 which is characterized by weak horizontal and vertical shear (Piani and Norton, 2002),

29 thereby allowing complicated structures to remain unmixed for long time periods. The rather

30 quiescent summer polar vortex can be contrasted with the winter polar vortex, in which large-

31 scale irreversible mixing may occur in the presence of upward propagating Rossby waves

32 (McIntyre and Palmer, 1983, 1984). The summer easterlies effectively block the upward

1   propagation of these waves (Charney and Drazin, 1961) and the flow becomes nearly zonally

2   symmetric. Hess (1991) used general circulation model (GCM) simulations of the final

3   warming of 1979 and Nimbus 7 Limb Infrared Monitor of the Stratosphere (LIMS) ozone

4   observations to show gradual homogenization of long-lived chemical tracers with the

5   background over the course of several months. Similar results were obtained with SLIMCAT

6   simulations of N_2O in the 1998 Arctic spring/summer by Orsolini (2001).

7   The situation cannot be entirely described by kinematic processes, however. Hess and Holton

8   (1985) and Hess (1991) describe the process whereby the tracer anomalies are initially

9   correlated with the winter polar vortex identified by potential vorticity (PV) anomalies, or

10   "vortices". The vortices, which are resistant to weak wind shear, protect the tracer anomalies

11   from stretching into elongated streaks and mixing irreversibly. The vortices eventually decay

12   due to radiative effects, thereby decorrelating PV from the chemical tracer. The chemical

13   tracer anomalies are then advected passively and eventually homogenize with the ambient air

14   due to shear-enhanced mixing. This two-stage process allows tracer structures to survive the

15   vigorous final warming process and the spin-up of the summer vortex. Waugh and Rong

16   (2002) examined the interannual variability of coherent PV structures that remain following

17   the breakup of the Arctic polar vortex, and they found that their longevity depends critically

18   on the timing of the breakup. In early breakup years (February and March), the vortex

19   remnants survive for around two months, while in late breakup years (late April and May), the

20   vortex remnants disappear quickly. In contrast to the protecting influence of vortices,

21   evanescent planetary waves in the lower stratosphere (below ~25 km) can enhance tracer

22   structure in the summer (e.g., Hoppel et al., 1999; Wagner and Bowman, 2000). The tracer

23   patterns in this region are not simply "frozen-in", but have a dynamical source. However, in

24   the middle-to-upper stratosphere (above ~25 km), where the feature discussed in this paper

25   resides, these waves are not likely to play a large role.

26   Most of the work to date has focused on the persistence and eventual homogenization of

27   winter polar vortex remnants in the summer stratosphere. This homogenization process is

28   important for setting up the fall trace gas distribution in the stratosphere (Durry and

29   Hauchecorne, 2005). However, recent work has uncovered convincing evidence for persistent

30   summer polar vortex anomalies of a different type. As explained by Lahoz et al. (2007), an

31   important class of anomalies involve so-called Frozen-In Anticyclones (FrIACs), i.e., long-

32   lived anticyclones originating from low latitudes, in contrast to winter polar vortex remnants,

1   i.e., long-lived cyclones originating from high latitudes. The FrIAC was first identified in

2   Aura Microwave Limb Sounder (MLS) data from March–August 2005. Manney et al. (2006,

3   hereinafter M06) describe how anomalies of high N_2O and low H_2O were pulled from the

4   tropics to high latitudes and became embedded in an anticyclone that formed in late March.

5   These chemical tracer anomalies persisted throughout the summer, circling westward around

6   the pole until late August. M06 searched for FrIAC-like signatures in PV fields for other

7   years and found several possibilities in 1982, 1994, 1997, 2002, and 2003. Global maps of

8   long-lived chemical tracer fields are unavailable for verification except in 2003. Indeed, a

9   second FrIAC event was observed in PV and Michelson Interferometer for Passive

10   Atmospheric Sounding (MIPAS) methane data during the summer of 2003 (Lahoz et al.,

11   2007). This FrIAC developed during the mid-April 2003 final warming and lasted (in the

12   chemical tracer field) until August. Lahoz et al. (2007) examined the FrIAC using pole-

13   centered cross-sections along the MIPAS orbit tracks. They identified a W-shaped pattern in

14   the methane field, which was caused by high values at polar latitudes that countered the

15   generally downward and poleward sloping isopleths. Although this pattern was initially

16   established by the poleward advection that resulted in the FrIAC, diabatic processes in the

17   summer may have helped to reinforce the feature.

18   It has been challenging to produce a credible simulation of the lifecycle of the 2005 FrIAC.

19   M06 used the SLIMCAT chemistry and transport model (CTM) (Chipperfield, 1999) driven

20   by U. K. Meteorological Office analyses to study the 2005 FrIAC. SLIMCAT produced the

21   early stages of the FrIAC, but the feature dissipated in late-May and June, two months early.

22   Reverse trajectory calculations also showed unrealistic shredding, suggesting deficiencies in

23   summer high-latitude winds. Since the M06 simulations there have been substantive

24   improvements in wind fields produced by assimilation systems and the use of that information

25   in the CTM framework. This paper presents 2-D (horizontal) and 3-D simulations of the 2005

26   event, both to enhance our understanding of the physical nature of the FrIAC as well as to test

27   current modeling capability of the summer polar circulation. The FrIAC provides an

28   excellent natural experiment of a robust, long-lived coherent tracer structure that is both

29   interesting and challenging to model. Section 2 describes the observational data (dynamical

30   fields and chemical tracers) used in this study. Section 3 details the simulations used to

31   reproduce the FrIAC. Section 4 presents the results, partitioning the FrIAC lifecycle into

32   three phases: spin-up phase (March to early April); anticyclonic phase (early April to May);

33   and shearing phase (June to August). Section 5 provides a summary and conclusions.

2 Observational Data

2.1 Meteorological Data

The meteorological dataset used for the dynamical fields in this study is the Goddard Earth Observing System Version 5.10 (GEOS-5) analysis from NASA's Global Modeling and Assimilation Office (GMAO), described by Reinecker et al. (2008). GEOS-5 uses the Gridpoint Statistical Analysis method of Wu et al. (2002), a 3D-Variational system, and a six-hour analysis window. The interface between the observations and the Global Circulation Model (GCM) is performed using the incremental analysis update (IAU) approach (Bloom et al., 1996), which avoids shocking the model, thus producing smoother analyses. GEOS-5 analyses are provided on 72 model levels from the surface to 0.01 hPa (75 km), on a 1/2° latitude by 2/3° longitude grid. The GEOS-5 PV and geopotential height are interpolated vertically to six isentropic surfaces for use in this study (580, 650, 740, 850, 960, and 1100 K). The Modern Era Retrospective-Analysis for Research and Applications (MERRA) reanalysis is also used for the Replay simulation described in Section 2.3. MERRA is a reanalysis from 1979 to the present, which uses the GEOS-5 data assimilation system (Version 5.20) throughout, providing a consistent analysis that includes online bias correction for satellite radiance observations (see http://gmao.gsfc.nasa.gov/merra for details).

2.2 Microwave Limb Sounder Data

The EOS Aura MLS measures millimeter- and submillimeter-wavelength thermal emission from the limb of Earth's atmosphere. Detailed information on the measurement technique and the MLS instrument on the EOS Aura satellite are given in Waters et al. (2006). The Aura MLS fields-of-view point in the direction of orbital motion and vertically scan the limb in the orbit plane, leading to data coverage from 82°S to 82°N latitude on every orbit. Vertical profiles are measured every 165 km along the suborbital track and have a horizontal resolution of ~200–300 km along-track and ~39 km across track. We use version 2.2 N_2O; validation of which is discussed by Lambert et al. (2007). Vertical resolution of the N_2O data is ~4 km for the region of interest in this study (approximately 30–3 hPa). For maps, MLS data are gridded using spatially weighted averages of each day's data in the region around each gridpoint on a 2.0° latitude by 5.0° longitude grid. Data values in the region not

1   observed by MLS (polewards of 82°N) are calculated by interpolating over the polar region

2   from neighboring grids. This is necessary for initializing VITA with complete global maps.

3   **3   Models**

4   **3.1 Three-Dimensional Chemistry and Transport Models**

5   Results are presented from two different three-dimensional simulations based on the Global

6   Modeling Initiative (GMI) Chemistry and Transport Model (hereinafter, GMI) and the GEOS-

7   5/MERRA Replay model (hereinafter, Replay). The GMI advection core uses a modified

8   version of the flux form semi-Lagrangian numerical transport scheme (Lin and Rood, 1996).

9   The meteorological fields in GMI are updated every 3 hours. The "G5Aura" simulation that is

10   presented in this study uses the 'Combo' chemical mechanism. 'Combo' combines the

11   stratospheric chemistry described in Douglass et al. (2004) with tropospheric chemistry from

12   the Harvard GEOS-CHEM model (Bey et al., 2001), as discussed in Strahan et al. (2007).

13   The horizontal resolution is 2.0° latitude by 2.5° longitude, while the vertical resolution in the

14   region of interest for this study (approximately 30–3 hPa) is ~1.1–1.5 km. Replay also uses

15   the Combo chemistry mechanism, but transport is computed using the GEOS-5 advection

16   core, a newer version of the flux form semi-Lagrangian numerical transport than used in GMI.

17   One noticeable difference that impacts this study is that the GEOS-5 advection core has an

18   improved implementation of polar transport compared with the current GMI transport scheme

19   via use of a smaller polar mixing cap (details are provided in Section 4.3). Replay uses

20   GEOS-5/MERRA analyzed meteorology, and also differs from the GMI in that it reads in

21   analyzed fields every 6 hours and then recomputes the analysis increments and physical

22   parameterizations every 30 minutes to update the meteorological fields.

23   **3.2 Van Leer Icosahedral Triangular Advection (VITA) 2-D Isentropic Transport**

24   **Model**

25   High-resolution simulations of the FrIAC were made with the Van leer Icosahedral Triangular

26   Advection (VITA) model, which solves the advection equation for a passive tracer on the

27   sphere using a finite-volume technique on a triangular grid (Allen and Nakamura, 2001,

28   2003). The finite-volume approach with a triangular grid is explained in Putti et al. (1990) for

29   equilateral triangles. Our approach differs from Putti et al. (1990) in two significant ways.

30   First, since it is not possible to cover the sphere with perfectly equilateral triangles, the VITA

1   grid uses non-equilateral triangles. Defining the triangle center for non-equilateral triangles is

2   ambiguous. We decided to use the circumcenter, defined as the intersection of the

3   perpendicular bisectors of the sides. This definition allows the center-to-side differences to be

4   easily calculated in determining the gradients. Attempts were made to limit the variation in

5   triangular size by shifting the locations of the nodes upon iteration. The current configuration

6   using 983040 triangles has a mean center-to-side distance of 9996 km, with a minimum

7   distance of 6,147 km (38% smaller) and maximum distance of 11,814 km (18% larger). The

8   nominal resolution is defined as twice the mean center-to-side distance or ~20 km. The

9   second difference is that the limiting function used in Putti et al. (1990), the so-called

10   "minmod" function, was replaced with the "superbee" function (Roe, 1985). The superbee

11   limiter provides less numerical diffusion, allowing sharper tracer gradients to be maintained

12   (Sweby, 1984). The VITA code is driven by offline winds (GEOS Version 5.10) at 24-hour

13   increments interpolated linearly in time and space to isentropic surfaces and to the

14   circumcenter of each triangle.

15   **4   Modeling the FrIAC**

16   **4.1   Overview of the 2005 Spring/Summer**

17   The winter-to-summer transition in the Arctic polar stratosphere is characterized by a reversal

18   of the mean zonal wind from westerly to easterly. This reversal occurs during the final

19   warming, with the precise timing varying from year to year (e.g., Waugh and Rong, 2002).

20   Figure 1a shows the zonal mean zonal wind at 850 K potential temperature (~32 km) for

21   March–August 2005 to provide an overview of this period. The winter polar vortex is

22   centered at around 65°N at the beginning of March and the zonal wind is increasing following

23   a minor warming in late February. A major warming occurs around March 10–15, with a

24   reversal to easterlies poleward of ~50°N (see line plot of zonal wind at 60°N in Figure 1b).

25   The easterlies decelerate in late March and return briefly to westerlies at 60°N before starting

26   a gradual easterly acceleration in April and May. The winds remain fairly steady during June

27   and July at this latitude, with peak values of around 12 m/s. The reversal to westerlies occurs

28   at the pole on 1 August and transitions steadily southward to reach 50°N by 1 September.

29   Although we show only 850 K level, the 2005 FrIAC extends from ~580 to 1100 K. The

1   zonal wind evolution at all levels throughout this height range is very similar to that shown

2   here in terms of the timing of the wind reversals.

3   The vertical lines drawn on Figure 1 relate to the three phases of the FrIAC described in the

4   subsequent sections. The first phase involves the spin-up of the FrIAC during March and early

5   April. The second phase refers to the period where the FrIAC can be identified by a coherent

6   anticyclone (early April–late May). The third phase (June–August) marks the time when the

7   chemical tracer signature of the FrIAC is gradually sheared by the background wind.

8   ## 4.2   Modeling the spin-up phase: March-early April

9   We first examine the spin-up of the 2005 FrIAC using PV and geopotential height in order to

10   highlight dynamical processes. Figure 2 shows Northern Hemisphere PV contours at 850 K,

11   overlaid with 10 hPa geopotential height (black lines), for select days during March 2005. On

12   1 March, the winter polar vortex (identified by high PV) is somewhat elongated and displaced

13   from the pole due to a strong Aleutian high (identified by black "H"). There are two

14   additional anticyclonic centers (identified by white "H"s) visible on this day with closed

15   height contours and low PV; one is off the coast of western Africa and the other is over Asia.

16   The Asian high remains stationary over the next several days, while the African high moves

17   eastward (counter clockwise) and merges with the Asian high, resulting in a strong Asian high

18   on 7 March. During this time, the Aleutian high weakens and the vortex moves back towards

19   the pole. The Asian high travels slowly eastward over the next three days and is approaching

20   the Aleutian high on 10 March. Together with the winter polar vortex and anticyclones, the

21   stratosphere develops a strong wave 2 pattern in the geopotential height on 13 March,

22   characteristic of the preconditioning phase of many major sudden warmings (Andrews et al.,

23   1987).

24   From 13–18 March, the two anticyclones merge into one large anticyclone. While this is

25   occurring, a tongue of low latitude, low PV air is advected along the poleward flank of the

26   now highly elongated winter polar vortex. This low PV air circulates around the Aleutian high

27   in a clockwise direction and becomes entrained into the Aleutian high by 23 March. The

28   winter polar vortex breaks into three distinct regions by 23 March (identified by lobes of high

29   PV), while another anticyclone is developing over Asia (identified by white "H"),

30   immediately eastward of the largest winter polar vortex remnant. From 23–25 March, this

31   developing anticyclone moves eastward and poleward and merges with the Aleutian high,

1 similar to the events of 13–18 March. A large tongue of low PV air stretches across northern

2 Asia on 25 March, indicating significant poleward transport. A portion of this tongue is

3 entrained into the Aleutian high so that by 28 March, the newly merged anticyclone is a

4 coherent entity at high latitudes that is vying for the polar position with the weakening main

5 polar vortex remnants. During this time, the extratropical wave motion is subsiding and the

6 FrIAC becomes a well-established feature in the polar circulation (identified by white "H" on

7 28 March).

8 Figure 3 illustrates the vertical extent of the FrIAC a week later, on 4 April, using PV maps

9 on multiple isentropic surfaces. Coherent PV anomalies are visible from 580 K to 1100 K

10 (~25-40 km), with correlated closed height contours indicating anticyclonic circulation. At

11 1300 K there appears to be more noise in the PV data and only a weak indication of a low PV

12 anomaly associated with one closed height contour. The FrIAC is observed to be vertically

13 upright at this stage with a horizontal width of approximately 20 degrees latitude (~2000 km)

14 across. So at this point, the FrIAC can be described as a coherent vortex ~15 km high and

15 ~2000 km wide embedded in the stratospheric flow. Later we will show that the FrIAC

16 remains vertically upright throughout April and most of May.

17 Given the characterization of the dynamical anomalies involved with the FrIAC, we now

18 examine observations and simulations of the chemical tracer anomalies that accompany the

19 spin-up phase. As shown by M06, MLS N_2O, H_2O and O_3 anomalies marked the location of

20 the FrIAC. We focus here on N_2O, since the GMI and Replay simulations do not have H_2O as

21 a prognostic variable in the stratosphere and since the O_3 anomaly decays in early April due to

22 photochemistry. Figure 4 shows the MLS N_2O evolution at 850 K, plotted for the same days

23 as Figure 2, along with Replay and VITA simulations. The VITA simulations were initialized

24 on 1 March using gridded MLS N_2O data and provide additional interpretation of high-

25 resolution features that are not resolvable by MLS, GMI, or Replay. Fine-scale filamentary

26 structures have been observed to cascade below the resolution of most Eulerian transport

27 models, down to a few kilometers in the horizontal (e.g., Flentje and Kiemle, 2003). The

28 horizontal scale of the VITA grid (~20 km) is larger than these observed filaments, suggesting

29 that features observed in VITA should be realistic. However, given that VITA is an isentropic

30 model, it neglects diabatic effects and vertical mixing processes and therefore some filaments,

31 particularly in regions of large vertical shear, may last longer than in the real atmosphere

32 (discussed further in Section 4.4).

1   The MLS data on 1 March show regions of high N_2O coinciding with the anticyclonic centers

2   over Asia and off the coast of Africa, indicating air of tropical origin. The MLS data also

3   show evidence of high N_2O tropical air that had previously been entrained into the Aleutian

4   high, a well-known process (Harvey et al., 1999). As the Asian and African anticyclones

5   merge on 7 March, the N_2O contours become wrapped up in a clockwise direction, as

6   observed in the high-resolution VITA simulation. As the Asian high moves eastward over the

7   next three days, the strong flow in-between the clockwise spinning Aleutian high and the

8   counter clockwise spinning winter polar vortex causes a thin tongue of air from the Asian

9   high to be drawn poleward on March 10 (marked by elevated N_2O in the Replay and VITA

10   simulations). By 13 March, this high N_2O air mixes into the Aleutian high. The winter polar

11   vortex on 13 March is comma-shaped, with the "head" of the comma poised for poleward

12   advection of tropical air. The result of this advection is visible on 18 March, when a long

13   ribbon of high N_2O air is drawn along the poleward flank of the now highly elongated vortex.

14   Some of this high N_2O air is eventually entrained into the Aleutian high, which has now

15   consolidated with the Asian high into one large anticyclone that by this time is centered close

16   to the pole. The VITA simulation on 23 March shows complicated swaths of high N_2O air

17   throughout the extratropical region, interwoven with low-N_2O air that originated in the winter

18   polar vortex.

19   From 23–25 March, both MLS and Replay show a large tongue of high N_2O air stretching

20   across northern Asia. The VITA simulation shows much finer detailed structure as this tongue

21   merges with elevated N_2O in the Aleutian high. By 28 March, the newly merged anticyclone

22   is vying for the polar position with the weakening main polar vortex remnant. These two

23   features are clearly marked by high/low N_2O values. The VITA simulation on 28 March has

24   generally higher background N_2O values than MLS or Replay. This may be due partly to the

25   VITA simulation being isentropic, while the diabatic circulation will pull down lower N_2O air

26   over the course of the month. However, the high resolution run does show numerous stripes

27   of low N_2O interwoven with high. The smoothing resulting from the retrieval and gridding

28   could account for the more uniform structure in the MLS data.

29   To examine this in more detail, Figure 5 provides slices through two Aura orbit tracks that

30   cross the center of the FrIAC on 28 March at 850 K. The locations of these tracks are

31   indicated by the white circles overlaid on polar plots of VITA and Replay N_2O. The VITA

32   and Replay N_2O are interpolated linearly in time and space to the locations of the MLS

1 observations for direct comparison. "Orbit 1" extends from left-to-right across the polar plots,

2 starting in the tropics and passing through the midlatitude "surf zone" in which VITA shows

3 complicated swaths of high and low N_2O. The line plots across this track (bottom left of

4 Figure 5) indicate higher variability of VITA N_2O in this region (profiles 25–45) compared

5 with MLS and Replay. This is expected, since the VITA simulations are at 20 km resolution,

6 while MLS data have a horizontal resolution of approximately 200–300 km along-track and

7 the meridional resolution for the Replay simulation is 2 degrees latitude (~220 km). The Orbit

8 1 track crosses the polar vortex around profile 45, indicated by the low N_2O values in the line

9 plots, before encountering the FrIAC from profiles 50-65. The peak value of the FrIAC

10 observed by MLS (~200 ppbv) is similar in the VITA simulation, but is lower in Replay

11 (~135 ppbv). As we will show, this is due to a low bias in the tropical N_2O in the Replay

12 simulations. From profiles 70–80 MLS encounters a second region of elevated N_2O followed

13 by a remnant of the winter polar vortex. These are seen as high and low N_2O anomalies

14 centered around profiles 70 and 85, respectively. The track ends in the high-N_2O tropical

15 region.

16 The second track (Orbit 12) starts in the tropics and crosses the main remnant of the winter

17 polar vortex (profiles 40–60) before encountering the FrIAC (profiles 60–75). VITA shows

18 more complicated structure in the FrIAC due to the swirling contours of high/low N_2O, which

19 are not evident in either MLS or Replay. After leaving the FrIAC this orbit passes through

20 alternating regions of low and high N_2O originating from the winter polar vortex and tropics,

21 respectively (profiles 75–100). The Replay and VITA simulations for this region are in

22 qualitative agreement with the MLS data, although VITA shows a large spike at profile 85 not

23 visible in MLS.

24 To examine the vertical structure along these tracks, MLS and Replay "curtain plots" are

25 provided in Figure 6. In Orbit 1 the FrIAC spans profiles 50–65 with elevated MLS N_2O

26 extending from around 30–3 hPa, consistent with the vertical extent of the PV anomaly.

27 Replay shows similar location and extent of the FrIAC, although peak values are too low.

28 Replay also captures the structure of the tilting winter polar vortex remnant from profiles 70-

29 100. The curtain plots for the second track show similar vertical extent and magnitude of the

30 FrIAC as in the first track, with the Replay again having similar morphology of the main

31 features observed in MLS.

1   Another view showing the vertical extent of the FrIAC is provided via polar plots of N_2O on 4

2   April from 580–1100 K (Figure 7), which can be compared with the PV plots in Figure 4.

3   N_2O anomalies exist in the MLS data at all levels, although at 1100 K the data become rather

4   noisy. Neither GMI nor Replay has a coherent positive anomaly at 580 K and 1100 K, but

5   both show coherent anomalies from 650–960 K. The position and extent of the anomalies

6   agree with the MLS data, but in each case the maximum N_2O values in GMI and Replay are

7   too low. This low bias is due to differences in background N_2O gradients. Figure 8 plots

8   zonal mean N_2O from 650 to 960 K, averaged over 1-10 March, the period preceding the

9   poleward flow events that set up the FrIAC. The MLS data show higher N_2O near the equator

10   than the simulations, with Replay showing the largest low bias. Since the FrIAC develops

11   from relatively unmixed tropical air, we would expect from these plots that the peak GMI and

12   Replay values will be low. The VITA simulations in Figure 7 that are initialized with MLS

13   observations nicely capture the location and magnitude of the N_2O anomalies at all levels,

14   suggesting the spin-up process mainly involves isentropic flow. Complicated swirling

15   structure is observed at 850 and 960 K, highlighting the anticyclonic circulation of the FrIAC.

16   The success of the simulations in reproducing many of the fine-scale features in the polar

17   stratosphere attests to the high quality of both the implemented transport scheme as well as

18   the assimilated wind fields from GEOS-5 and MERRA.

19   ## 4.3   Modeling the Anticyclonic phase: early April-May

20   The second phase of the FrIAC is characterized by the existence of a coherent anticyclone

21   that meanders about the pole for approximately two months. The FrIAC during this phase can

22   still be identified by anomalously low PV and closed geopotential height contours. Figure 9

23   shows PV and geopotential height at 850 K for select days in April and May 2005.

24   Immediately following the spin-up phase, the FrIAC takes an interesting path directly across

25   the pole, as seen in the maps for 1, 7, and 14 April, where the PV anomaly moves from left to

26   right across the map (examined in more detail below). Following the polar crossing, from 14

27   April–5 May, the FrIAC travels westward completely around the pole; on 28 April it is

28   centered near 180° longitude and by 5 May moves to the Greenwich Meridian, similar to 14

29   April. By 5 May, the PV anomaly has noticeably weakened. In addition, the winter polar

30   vortex remnants, marked by high PV, have weakened as well, as expected due to radiative

31   processes (Hess, 1991). From 5–9 May the FrIAC makes a second polar-crossing (this time

32   from right to left across the maps on Figure 9) before continuing steady westward progression

1   around the pole. On 15 May, the PV anomaly is very weak, and by 30 May has completely

2   disappeared. The PV anomaly therefore lasted approximately two months after the winter

3   polar vortex breakup in late March, consistent with expectations for a late-March breakup of

4 · the northern winter vortex (Waugh and Rong, 2002).

5   Figure 10 presents the MLS, Replay, and VITA N_2O evolution at 850 K for the same days as

6   shown in Figure 9. For this phase, VITA was reinitialized on 1 April 2005 with MLS data.

7   This re-initialization allows a better direct comparison for this period by removing much of

8   the fine-scale structure that was generated in VITA during the polar vortex breakup (see

9   Figure 5). Also, this reinitialization removes any biases that develop due to lack of vertical

10   motion in VITA. The maps for 1 April show high N_2O air in the anticyclonic vortex. From

11   this point on we will continue to refer to the region of high N_2O as the Frozen-In Anticyclone

12   (FrIAC), although as seen in Figure 9, the feature isn't always identified by anticyclonic

13   circulation. From 1–7 April, the FrIAC moves eastward and poleward, with anticyclonic flow

14   that spins off several narrow streamers of high N_2O air as produced in the VITA simulation.

15   From 7–14 April, the FrIAC moves directly across the pole and becomes centered over

16   northern Greenland. This episode provides a useful test of the numerical representation of

17   cross-polar flow, which has posed problems for global models based on regular

18   latitude/longitude grids (Williamson, 2007). Early versions of GMI imposed a well-mixed

19   polar cap in order to dampen effects of noisy assimilated wind fields at the pole (Allen et al.,

20   1991). Although present meteorological fields are far less noisy than those available to Allen

21   et al. (1991), the GMI the polar cap still extends from 87° to the pole and is 6° (~660 km)

22   across. The Replay transport scheme applies the polar cap only over one grid cell, extending

23   from 89° to the pole, thereby decreasing the size of the cap by a factor of 9, substantially

24   reducing numerical diffusion associated with the larger polar cap.

25   The MLS data and simulations from GMI, Replay, and VITA for the cross-polar flow at 740

26   K are provided in Figure 11. On 8 April the N_2O anomaly starts to encounter the polar cap

27   region (identified by black circle in GMI and Replay). A small "bite-out" of the N_2O

28   maximum can be seen at the pole on this day in the GMI simulation. Two days later, a large

29   portion of the GMI N_2O anomaly has been reduced, and by 12 April the red contours,

30   indicating mixing ratios over ~150 ppbv have disappeared completely. The peak mixing ratio

31   during this period decreases by 22% from 172 to 133 ppbv in the GMI simulation. The

32   Replay simulation, on the other hand, shows a nearly constant N_2O peak as the FrIAC crosses

1   the pole. Only a very slight drop (~1%) is observed in this run, consistent with the nearly

2   constant peak in the MLS data. In hindsight, these results are to be expected, since

3   implementation with a polar cap of 660 km is unable to resolve a feature ~2000 km across.

4   The Replay polar cap is much smaller relative to the size of the FrIAC and therefore better

5   resolves the feature. In the remainder of the paper we focus on the Replay simulation, since

6   the FrIAC is significantly "washed out" in the GMI simulation after this event. Note that the

7   VITA simulation advects the FrIAC over the pole undiminished as there is no "pole-problem"

8   with the triangular grid.

9   During this time the easterly summer jet is accelerating (see Figure 1), so that around 14 April

10   the FrIAC starts its westward march around the pole, reaching 180°E longitude by 28 April

11   and back near the Greenwich Meridian on 5 May (Figure 10). Even though the feature is

12   advected westward around the pole, it still exhibits local anticyclonic rotation, with streamers

13   of high N_2O air drawn off equatorward (see Replay and VITA results for 28 April). After the

14   second polar crossing on 5–9 May, the FrIAC continues to circle the pole with a rotation

15   period of approximately 10–15 days, maintaining a central position at latitude around 70–

16   80°N.

17   On 15 May there is still a clear correspondence between the location of the geopotential

18   height maximum and the highest N_2O values. From 15–30 May, the geopotential height and

19   N_2O contours decouple, so that the FrIAC is no longer identified by anticyclonic rotation.

20   Starting at this point, the air marked by high N_2O mixing ratios is advected passively by the

21   circumpolar jet. The immediate result is that a large streamer of high N_2O air emerges from

22   the main core of the FrIAC around 15 May. This causes the FrIAC to diminish slightly in

23   size, but it is still the dominant feature at high latitudes. The Replay and VITA simulations

24   maintain close correspondence with MLS in terms of the location and size of the FrIAC,

25   albeit with lower maximum values in Replay and more structure in VITA. Aura along-track

26   cross-sections through the FrIAC at 850 K for 15 May are shown in Figure 12. The Replay

27   simulation agrees remarkably well with MLS for both tracks, capturing much of the large-

28   scale and fine-scale structure, with exception of the reduced magnitude of the peak. VITA

29   captures the magnitude of the peak, but shows more fine-scale structure than observed in

30   MLS, as expected. There are several valleys and peaks in VITA that don't exist in the MLS

31   data, such as the peak near profile 90 in Orbit 1 and the peaks near profiles 40 and 60 in Orbit

32   2.

1   The anticyclonic phase of the FrIAC is marked by both dynamical (local coherent anticyclone

2   and low PV) and chemical (high N_2O) signatures. The dynamical properties act to protect the

3   chemical tracer anomaly from the shearing effects of the wind. This is similar to the

4   protective nature of the winter polar vortex remnants that were discussed in Hess and Holton

5   (1985) and Hess (1991). In the case of the 2005 FrIAC the dynamical signature lasted

6   approximately two months, consistent with expected timescales of radiative damping. In the

7   next section we examine the fate of the chemical signature of the FrIAC as it becomes

8   exposed to the shearing effects of the summer vortex.

9   ## 4.4 Modeling the Shearing phase: June-August

10   The coherent structure of the main body of the FrIAC observed during the anticyclonic phase

11   suggests that the horizontal flow is nearly in solid body rotation (SBR), at least at the high

12   latitudes where the FrIAC develops, in agreement with Piani and Norton (2002). SBR occurs

13   when there is no meridional wind and the zonal wind is proportional to the cosine of latitude

14    $(u(\varphi) = u_{eq} \cos(\varphi)$, where u_{eq} is the equatorial wind speed and φ is latitude). In Figure 13, the

15   GEOS-5 zonal mean wind at 850 K is plotted for select days from April through August,

16   along with zonal wind for SBR with different periods of rotation (10, 20, 30, 40, and 50

17   days). In late April the flow is approaching SBR at high latitudes, with period of around 10

18   days (called SBR_{10} for short), while on May 10, the wind is very close to SBR_{10} from about

19   75–85°N, similar to the latitudinal extent of the FrIAC. The flow does not follow SBR

20   equatorward of 70°N in late May, consistent with the high-N_2O streamer that develops (see

21   Figure 10). From 30 June–20 July, the rotation more closely follows SBR_{20} from about 65–

22   90°N. By 10 August, the flow deviates from SBR with slower winds than required at polar

23   latitudes, suggesting that significant horizontal shearing of the FrIAC will occur in August.

24   As the winds reverse to westerly the SBR rotation completely breaks down, as seen on 25

25   August. These wind analyses show that quasi-SBR occurs at high latitudes thoughout most of

26   May, June, and July at 850 K, but breaks down completely in mid- to late-August. A high-

27   latitude feature in the tracer field would thus be expected to survive the flow over several

28   months, barring effects of vertical shear (examined in more detail below).

29   The vertical structure of the FrIAC for MLS and Replay is shown in Figure 14, which plots

30   the zonal N_2O anomaly at 74°N as a function of longitude and pressure for select days in May

31   and June 2005. On 1 and 22 May the FrIAC (marked by high N_2O) is upright, whereas the

1   background N_2O contours show significant vertical tilting (westward with height),

2   particularly in Replay. Dynamical studies show that coherent vortices can exhibit resistance to

3   the tilting effects of weak vertical shear. Vandermeirsh and Morel (2002), using a 2 ½ layer

4   quasigeostrophic model, with separate PV anomalies in each layer, show that the PV

5   anomalies have a self-sustaining advective effect on the other layer that keeps the vortex from

6   splitting in weak shear zones. A more detailed study (Jones, 1995), using primitive-equation

7   numerical modeling of a tropical tropospheric cyclone in vertical shear, shows that upper and

8   lower PV anomalies of an initially barotropic vortex rotate about a common center. The

9   effects of this rotation act to oppose the destructive action of the vertical shear on the vortex.

10   Further work is necessary to elucidate whether these results are consistent with this

11   anticyclonic vortex in the polar stratosphere. As the PV anomaly decays in late May,

12   however, the FrIAC starts tilting and weakening, as observed on 28 May, with even further

13   tilting occurring in June, described in more detail below.

14   Figure 15 shows the evolution of MLS, Replay, and VITA N_2O at 850 K for select days

15   during June–August 2005. VITA was again reinitialized for this period using MLS data on 1

16   June. In early June, the FrIAC exhibits evidence of horizontal shearing. Whereas on 1 June

17   the main cell of the FrIAC is nearly circular in shape and centered on the Greenwich Meridian

18   near 80°N, by 10 June the feature has elongated in the zonal direction due to weak meridional

19   shear of the zonal wind. Note the long tail that lags behind the main cell of the FrIAC at

20   lower latitudes on 10 June, evident in MLS data and the simulations. By 20 June, the main

21   part of the FrIAC has moved westward to 180°E, and the elongated tail wraps completely

22   around the globe. By 30 June, the FrIAC is again over the Greenwich Meridian and is now in

23   a horseshoe-shaped configuration with a main cell and two outstretched arms. Starting in early

24   July, noticeable differences occur between VITA and MLS data. On 15 July the high N_2O

25   region in the VITA simulation is spread over 180 degrees of longitude in a rather complicated

26   structure. The MLS data on this date show a single region of high N_2O near the pole,

27   immersed in background N_2O levels that are somewhat higher than at midlatitudes. It is

28   unlikely that smoothing of the MLS data can completely account for these differences. To

29   examine this further, Figure 16 presents along-track plots for 15 July through the large N_2O

30   anomaly observed in VITA. In Orbit 1 the large anomaly observed in the VITA simulation

31   (profiles 45-60) doesn't have a counterpart in either MLS or Replay. In Orbit 2 there is an

32   anomaly in MLS, but it is observed at a slightly different location.

1   From 15 July to 30 August, MLS shows the FrIAC to be slowly dissipating (Figure 15),

2   mixing with the background N_2O levels. M06 examined SLIMCAT and Reverse-Trajectory

3   (RT) simulations of the FrIAC and found that unrealistic shredding of the feature occurred in

4   the simulation, suggesting that the analyzed horizontal winds (U. K. Met Office in their case)

5   are unrealistically dispersive at high latitudes in summer. However, the Replay results show

6   remarkably good agreement with MLS during this third phase, matching the morphology of

7   the N_2O contours well through at least 15 August. This suggests that the MERRA winds and

8   Replay transport scheme are able to reliably capture the transport of the summer middle

9   stratosphere. Complete mixing of the FrIAC in Replay does not occur until late August, when

10   the feature has all but disappeared in the MLS data as well. Note that the elevated N_2O

11   observed in MLS data on 30 August near 90°E and just off the pole is a new feature that was

12   not formed by the FrIAC, but the feature at 180° longitude is the final observable remnant of

13   the FrIAC, indicating that complete mixing of the FrIAC may not occur before the winter

14   vortex becomes established in September. That the VITA simulation shows considerable

15   structure in late August suggests that it is largely vertical shear (neglected in VITA) rather

16   than horizontal shear that acts to dissipate the FrIAC. We will attempt to quantify the relative

17   importance of horizontal and vertical shearing effects below.

18   To summarize performance of the simulations over the entire FrIAC lifecycle, Figure 17

19   presents Hovmöller (longitude vs. time) diagrams of the observed and modelled N_2O at 850 K

20   and 78°N from March–August 2005. The MLS data show that after spin-up the FrIAC makes

21   seven complete cycles around the pole from April to August. The amplitude of the N_2O

22   anomaly remains relatively undiminished until late July, when the FrIAC apparently develops

23   two maxima around this latitude circle. In August, the westward motion slows significantly,

24   becoming nearly stationary in the latter part of the month. During this time the maximum

25   N_2O values diminish and the feature mixes into the background. The simulations capture

26   many of the features observed in MLS. The polar-crossings on 7–14 August and 5–9 May are

27   evident in Replay and GMI as temporary disappearances of the N_2O anomaly at 78°N, as the

28   feature is poleward of this latitude. The GMI simulation shows sharply diminished peak

29   values during these crossings, leaving a very weak N_2O anomaly in mid-May. However,

30   following the second polar crossing GMI shows relatively undiminished N_2O anomaly for

31   four complete cycles. This suggests the analyses and transport schemes are able to maintain

32   the structure of the FrIAC during this period. This is further attested by the Replay simulation,

33   which captures the entire FrIAC lifecycle at this level both qualitatively and quantitatively.

1   Since it is able to resolve the feature during the polar crossings, the N_2O anomaly is higher in

2   mid-May than in GMI. The anomaly remains undiminished throughout May, June, and July,

3   and even shows a similar splitting into two anomalies in late July, as seen in the MLS data. In

4   August, the Replay continues to capture the anomaly until it diffuses into the background by

5   the end of the month. Replay contours of 75 and 100 ppbv are overlaid on the MLS contours

6   in Figure 17 for comparison. As seen by the close correspondence with MLS, Replay

7   performs remarkably well at simulating the evolution and decay of the FrIAC.

8   The VITA simulation is also shown for comparison. As discussed previously, VITA tends to

9   generate complex structures in the tracer field that last longer than in the MLS observations,

10 due to better horizontal resolution. The Hovmöller plot shown here uses a composite of

11 VITA runs that are initialized on 1 March, 1 April, and 1 June, respectively, in order to reduce

12 the build-up of these features. Even so, more detailed structure occurs in the VITA simulation

13 than seen in the MLS data or the other simulations. Particularly during August, the VITA

14 simulation shows considerable structure. This highlights the fact that vertical processes

15 (neglected in VITA) are necessary for complete modelling of the FrIAC.

16 That Replay is able to simulate the remnants of the FrIAC well into August implies that the

17 implemented vertical and horizontal resolution is adequate to capture the details of the feature

18 during the shearing phase, at least to the resolution of MLS. Vertical shear during the June-

19 August period causes significant tilting of the tracer structures that decreases the vertical scale

20 and enhances vertical mixing as explained by Haynes and Anglade (1997). To quantify this

21 scale reduction, we employ a simple model to estimate the time for the vertical scale of the

22 FrIAC to reduce to the implemented grid scale (~1 km for Replay). The N_2O cross-sections

23 in Figure 14 suggest that we can approximate the FrIAC as a rectangular tracer anomaly with

24 horizontal length (in the zonal direction) H and vertical depth D embedded in a zonal flow

25 with vertical shear (see schematic in Figure 18). We can calculate the vertical depth D' of the

26 anomaly after the top has completely cleared the base by $D'/H = D/[(u_2 - u_1)T]$, where T is

27 the time elapsed. Using the approximate vertical shear in zonal wind at 75°N and 10 hPa

28 ($\sim0.4 \text{ ms}^{-1} \text{ km}^{-1}$ or 0.0004 s^{-1} in late June/early July) and horizontal scale ~2000 km we

29 obtain a time-scale of ~60 days to reduce the FrIAC to ~1 km. This suggests that GMI should

30 resolve the vertical features of the FrIAC for around two months during the shearing phase,

31 consistent with results presented here. Similar arguments can be used to estimate the time-

32 scale for horizontal shear to reduce the lateral scale of the FriAC to that of the GMI resolution

1   (2°). Using the lateral shear in the zonal wind (~0.5° longitude/day/°latitude in June and July)

2   along with a zonal width of 100° we estimate that the FrIAC will be resolvable by GMI for

3   ~100 days. That Replay simulates the horizontal structure of the FrIAC throughout the June–

4   August shearing phase is consistent with these rough estimates.

5   The FrIAC provides an excellent case study for examining chemical tracer evolution in weak

6   shear flows. Given its coherent nature, it is easy to discriminate air within the FrIAC over the

7   course of five months. The Replay simulates the structure of the FrIAC in N_2O over its entire

8   lifecycle, at least to the resolution of MLS, attesting both to the assimilated wind fields, the

9   numerical transport, and the simulated N_2O destruction.

10 **5   Summary and Conclusions**

11 The general process whereby complicated tracer structures are frozen into the relatively

12 quiescent summer easterly stratospheric flow has been understood for some time. However,

13 detailed observational analysis of long-lived anticyclones such as the 2005 FrIAC over the

14 course of the entire summer depended on the availability of daily hemispheric observations of

15 long-lived tracers such as N_2O and H_2O. This study used MLS observations and chemistry

16 and transport simulations to make a detailed analysis of the lifecycle of the FrIAC. The spin-

17 up of the FrIAC occurred when the winter polar vortex was displaced off the pole by the

18 major final warming, causing low latitude air to move northward and merge with the Aleutian

19 high. This process involved two separate episodes that resulted in a coherent anticyclone at

20 very high latitudes, which became enveloped by the summer easterly flow. The anticyclone

21 traversed the pole once in mid-April and once in mid-May before starting a regular westward

22 propagation over the next three months. Until the anticyclone decayed in late May, it

23 protected the FrIAC from vertically shearing. The FrIAC then underwent a regular westward

24 rotation from June–August. Horizontal and vertical shearing in June and July caused the

25 FrIAC to stretch and start to mix with the background air. The FrIAC was finally torn apart in

26 August, although remnants were observed as late as the end of August, when winds became

27 westerly over the entire polar region. Calculations of the shear-induced reduction of vertical

28 and horizontal scales of the FrIAC are consistent with the feature lasting for several months

29 during the shear phase.

30 Simulations produced using the GMI with GEOS-5 analyses follow the behavior of the FrIAC

31 longer than SLIMCAT simulations presented in M06, but the feature becomes largely

1 indistinguishable by early July. Isentropic simulations using VITA reproduce many aspects of

2 the FrIAC, but small-scale structures maintained by VITA that are not found in MLS are

3 problematic and show that important mixing processes are absent from this simple single-

4 level simulation. Some improvement in the VITA representation of the FrIAC is gained by

5 periodic re-initialization, suggesting that the information to produce a credible FrIAC

6 simulation is present in the analyses and that GEOS-5 fields themselves do not cause the poor

7 comparisons of MLS observations with GMI. Analysis shows that the comparisons between

8 observations and GMI simulation become markedly worse whenever the FrIAC is transported

9 over the pole.

10 Results from a simulation with improved horizontal resolution at the pole support this

11 conclusion. The Replay simulation reproduces the important features of the FrIAC, including

12 its August demise. An important difference between the GMI and Replay is the size of the

13 well-mixed polar cap. The large (3° latitude radius) polar cap, used in early implementations

14 to keep the transport code stable when using the noisy assimilated wind fields common to that

15 era, was used in the GMI simulations. The FrIAC horizontal scale is only ~2000 km

16 compared to the diameter of the polar cap (660 km), thus any simulation that assumes a well

17 mixed polar cap of this size cannot maintain a feature the size of the FrIAC if it is transported

18 across the pole, whereas the Replay with 1° polar cap performed remarkably well. Replay also

19 simulated the final mixing processes of the FrIAC well into August, suggesting that the

20 vertical and horizontal resolutions are sufficient to resolve the main aspects of the feature.

21 The success of the Replay is very encouraging with respect to current state-of-the-art models

22 and meteorological analyses.

30

References

Allen, D. J., Douglass, A. R., Rood, R. B., and Guthrie, P. D.: Application of a monotonic upstream-biased transport scheme to three-dimensional constituent transport calculations, Mon. Wea. Rev., 119, 2456–2464, 1991.

Allen, D. R., and Nakamura, N.: A seasonal climatology of effective diffusivity in the stratosphere, J. Geophys. Res., 106, 7917–7936, 2001.

Allen, D. R., and Nakamura, N.: Tracer equivalent latitude: A diagnostic tool for isentropic transport studies, J. Atmos. Sci., 60, 287–304, 2003.

Andrews, D. G., Holton, J. R., and Leovy, C. B.: Middle Atmosphere Dynamics, Academic Press, Inc., Orlando, Florida, 1987.

Bey, I., Jacob, D. J., Yantosca, R. M., Logan, J. A., Field, B. D., Fiore, A. M., Li, Q., Liu, H. Y., Mickley, L. J., and Schultz, M. G.: Global modeling of tropospheric chemistry with assimilated meteorology: Model description and evaluation, J. Geophys. Res., 106, 23,073–23,095, 2001.

Bloom, S. C., Takacs, L. L., da Silva, A. M., and Ledvina, D.: Data assimilation using incremental analysis updates, Mon. Weather Rev., 124, 1256–1271, 1996.

Charney, J. G., and Drazin, P. D.: Propagation of planetary-scale disturbances from lower into upper atmosphere, J. Geophys. Res., 66, 83–109, 1961.

Chipperfield, M. P.: Multiannual simulations with a three-dimensional chemical transport model, J. Geophys. Res., 104, 1781–1805, 1999.

Douglass, A. R., Stolarski, R. S., Strahan, S. E., and Connell, P. S.: Radicals and reservoirs in the GMI chemistry and transport model: Comparison to measurements, J. Geophys. Res., 109, D16303, doi:10.1029/2004JD004632, 2004.

Durry, G., and Hauchecorne, A.: Evidence for long-lived polar vortex air in the mid-latitude summer stratosphere from in situ laser diode CH_4 and H_2O measurements, Atmos. Chem. Phys., 5, 1467–1472, 2005.

Flentje, H., and Kiemle, C.: Erosion and mixing of filaments in the arctic lower stratosphere revealed by airborne lidar measurements, J. Geophys. Res., 108, 4232, doi:10.1029/2002JD002168, 2003

Harvey, V. L., Hitchmann, M. H., Pierce, R. B., and Fairlie, T. D.: Tropical aerosol in the Aleutian high, J. Geophys. Res., 104, 6281–6290, 1999.

Haynes, P., and Anglade, J.: The vertical-scale cascade in atmospheric tracers due to large-scale differential advection, J. Atmos. Sci., 54, 1121–1136, 1997.

Hess, P. G., and Holton, J. R.: The origin of temporal variance in long-lived tracer constituents in the summer stratosphere, J. Atmos. Sci., 42, 1455–1463, 1985.

Hess, P. G.: Variance in trace constituents following the final stratospheric warming, J. Geophys. Res., 95, 13,765–13,779, 1990.

Hess, P. G.: Mixing processes following the final stratospheric warming, J. Atmos. Sci., 48, 1625–1641, 1991.

Hoppel, K. W., Bowman, K. P., and Bevilacqua, R. M.: Northern Hemisphere summer ozone variability observed by POAM II, Geophys. Res. Lett., 26, 827–830, 1999.

Jones, S. C.: The evolution of vortices in vertical shear. I: Initially barotropic vortices, Q. J. R. Meteorol. Soc., 121, 821–851, 1995.

Lahoz, W. A., Geer, A. J., and Orsolini, Y. J.: Northern hemisphere stratospheric summer from MIPAS observations, Q. J. R. Meteorol. Soc., 133, 197–211, 2007.

Lambert, A., Read, W. G., Livesy, N. J., Santee, M. L., Manney, G. L., Frodevaux, L., Wu, D. L., Schwartz, M. J., Pumphrey, H. C., Jimenez, C., Nedoluha, G. E., Cofield, R. E., Cuddy, D. T., Daffer, W. H., Drouin, B. J., Fuller, R. A., Jarnot, R. F., Knosp, B. W., Pickett, H. M., Perun, V. S., Snyder, W. V., Stek, P. C., Thurstans, R. P., Wagner, P. A., Waters, J. W., Jucks, K. W., Toon, G. C., Stachnik, R. A., Bernath, P. F., Boone, C. D., Walker, K. A., Urban, J., Murtagh, D., Elkins, J. W., and Atlas, E.: Validation of the Aura Microwave Limb Sounder middle atmosphere water vapor and nitrous oxide measurements, J. Geophys. Res., 113, D24S36, doi:10.1029/2007JD008724, 2007.

Lin, S.-J., and Rood, R. B.: Multidimensional flux-form semi-Lagrangian transport schemes, Mon. Wea. Rev., 124, 2046–2070, 1996.

Manney, G. L., Livesy, N. J., Jimenez, C. J., Pumphrey, H. C., Santee, M. L., MacKenzie, I. A., and Waters, J. W.: EOS Microwave Limb Sounder observations of frozen-in anticyclonic air in Arctic summer, Geophys. Res. Lett., 34, L06810, doi:10.1029/2005GL025418, 2006.

McIntyre, M. E., and Palmer, T. N.: Breaking planetary-waves in the stratosphere, Nature, 305, 593–600, 1983.

McIntyre, M. E., and Palmer, T. N.: The surf zone in the stratosphere, J. Atmos. Terr. Phys., 46, 825–849, 1984.

Orsolini, Y. J.: Long-lived tracer patterns in the summer polar stratosphere, Geophys. Res. Lett., 28, 3855–3858, 2001.

Piani, C., and Norton, W. A.: Solid-body rotation in the northern hemisphere summer stratosphere, Geophys. Res. Lett., 29, 2117, doi:10.1029/2002GL016079, 2002.

Putti, M., Yeh, W.-G., and Mulder, W. A.: A triangular finite volume approach with high-resolution upwind terms for the solution of groundwater transport equations, Water Resources Research, 26, 2865–2880, 1990.

Reinecker, M. M., Suarez, M. J., Todling, R., Bacmeister, J., Takacs, L., Liu, H.-C., Gu, W., Sienkiewicz, M., Koster, R. D., Gelaro, R., Stajner, I., and Nielsen, J. E.: The GEOS-5 data assimilation system: Documentation of Versions 5.0.1, 5.1.0, and 5.2.0, NASA Tech. Rep. 104606, Vol. 27, 2008.

Roe, P. L.: Some contributions to the modeling of discontinuous flows, in: Lecture Notes in Applied Mathematics, 22, 163–193, New York: Springer-Verlag, 1985.

Strahan, S. E., Duncan, B. N., and Hoor, P.: Observationally derived transport diagnostics for the lowermost stratosphere and their application to the GMI chemistry and transport model, Atmos. Chem. Phys., 7, 2435-2445, doi:10.5194/acp-7-2435-2007, 2007.

Sweby, P. K.: High resolution schemes using flux limiters for hyperbolic conservation laws, SIAM J. Numer. Anal., 21, 995–1011, 1984.

Vandermeirsh, F., and Morel, Y.: Resistance of a coherent vortex to a vertical shear, J. Phys. Oceanogr., 32, 3089–3100, 2002.

Wagner, R. E., and Bowman, K. P.: Wavebreaking and mixing in the Northern Hemisphere summer stratosphere, J. Geophys. Res., 105, 24,799–24,807, 2000.

Waters, J.W., Froidevaux, L., Harwood, R.S., Jarnot, R.F., Pickett, H.M., Read, W.G., Siegel, P.H., Cofield, R.E., Filipiak, M.J., Flower, D.A., Holden, J.R., Lau, G.K.K., Livesey, N.J., Manney, G.L., Pumphrey, H.C., Santee, M.L., Wu, D.L., Cuddy, D.T., Lay, R.R., Loo, M.S., Perun, V.S., Schwartz, M.J., Stek, P.C., Thurstans, R.P., Boyles, M.A., Chandra, K.M.,

1   Chavez, M.C., Chen, G.S., Chudasama, B.V., Dodge, R., Fuller, R.A., Girard, M.A., Jiang,

2   J.H., Jiang, Y.B., Knosp, B.W., LaBelle, R.C., Lam, J.C., Lee, K.A., Miller, D., Oswald, J.E.,

3   Patel, N.C., Pukala, D.M., Quintero, O., Scaff, D.M., Van Snyder, W., Tope, M.C., Wagner,

4   P.A., and Walch, M.J.: The Earth Observing System Microwave Limb Sounder (EOS MLS)

5   on the Aura satellite, IEEE Trans. Geosci. Remote Sens., 44, 1075–1092, 2006.

6   Waugh, D. W., and Rong, P. P.: Interannual variability in the decay of lower stratospheric

7   Arctic vortices, J. Meteor. Soc. Japan, 80, 997–1012, 2002.

8   Williamson, D. L.: The evolution of dynamical cores for global atmospheric models, J.

9   Meteor. Soc. Japan, 85B, 214–269, 2007.

10 Wu, W.-S., Purser, R. J., and Parish, D. F.: Three-dimensional analyses with spatially

11 inhomogeneous covariances, Mon. Weather Rev., 130, 2905–2916, 2002.

12

(a) Zonal Mean Zonal Wind at 850 K

(b) Zonal Mean Wind at 60 N
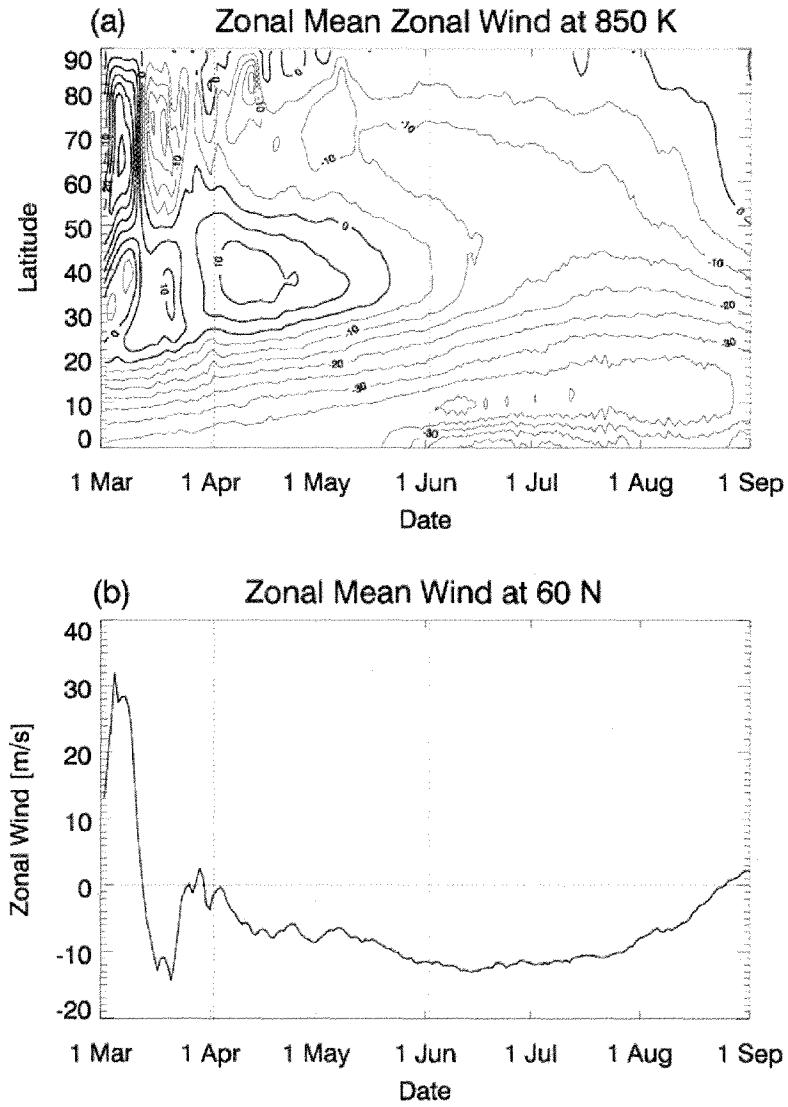
Figure 1. (a) Zonal mean zonal wind at 850 K potential temperature for March–August 2005.
(b) Zonal mean zonal wind at 850 K potential temperature and 60°N latitude for March–
August 2005. Vertical dotted lines indicate transitions between the three phases of the FrIAC
(see text for details).
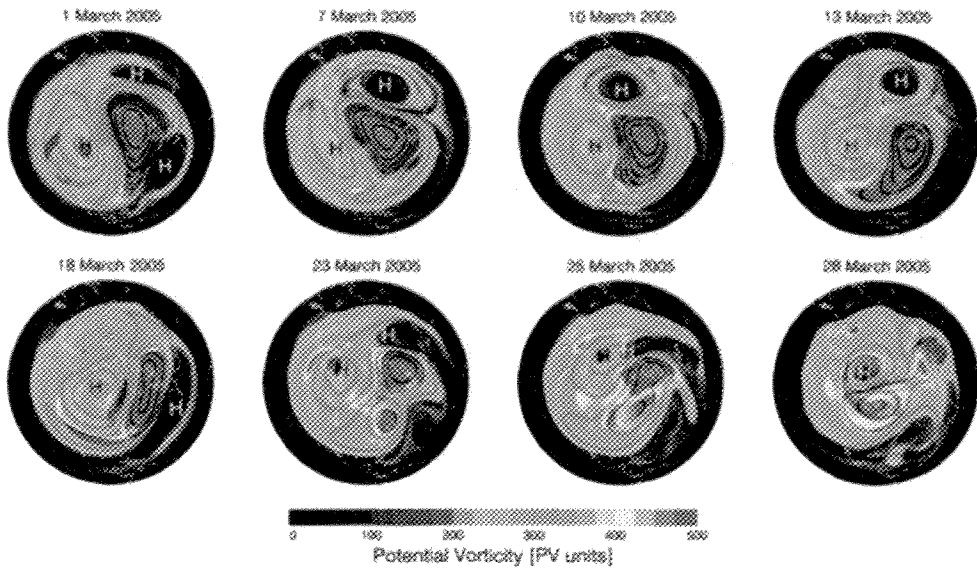
1

2 Figure 2. Northern Hemisphere Ertel potential vorticity at 850 K potential temperature for

3 select days in March 2005 (colored contours). PV units are used, where 1 PVU = 1.0×10^{-6}

4 $m^2 \, s^{-1} \, K \, kg^{-1}$. Black lines indicate 10 hPa geopotential height at 25-m contour intervals. The

5 black "H" marks the location of the Aleutian anticyclone and the white "H"s mark the

6 locations of other anticyclones.

7
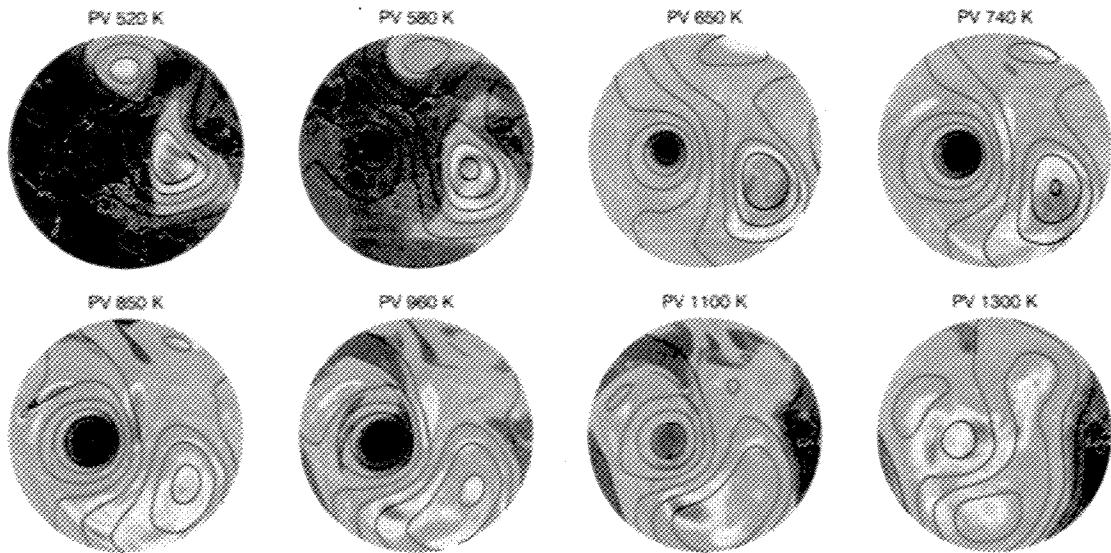
Figure 3. Ertel potential vorticity at multiple potential temperature levels from 50–90°N on 4 April 2005. Contour colors are scaled to the range of PV values for the given level, with red (black) indicating high (low) PV. White lines show 10 hPa geopotential height at 10-m contour intervals.
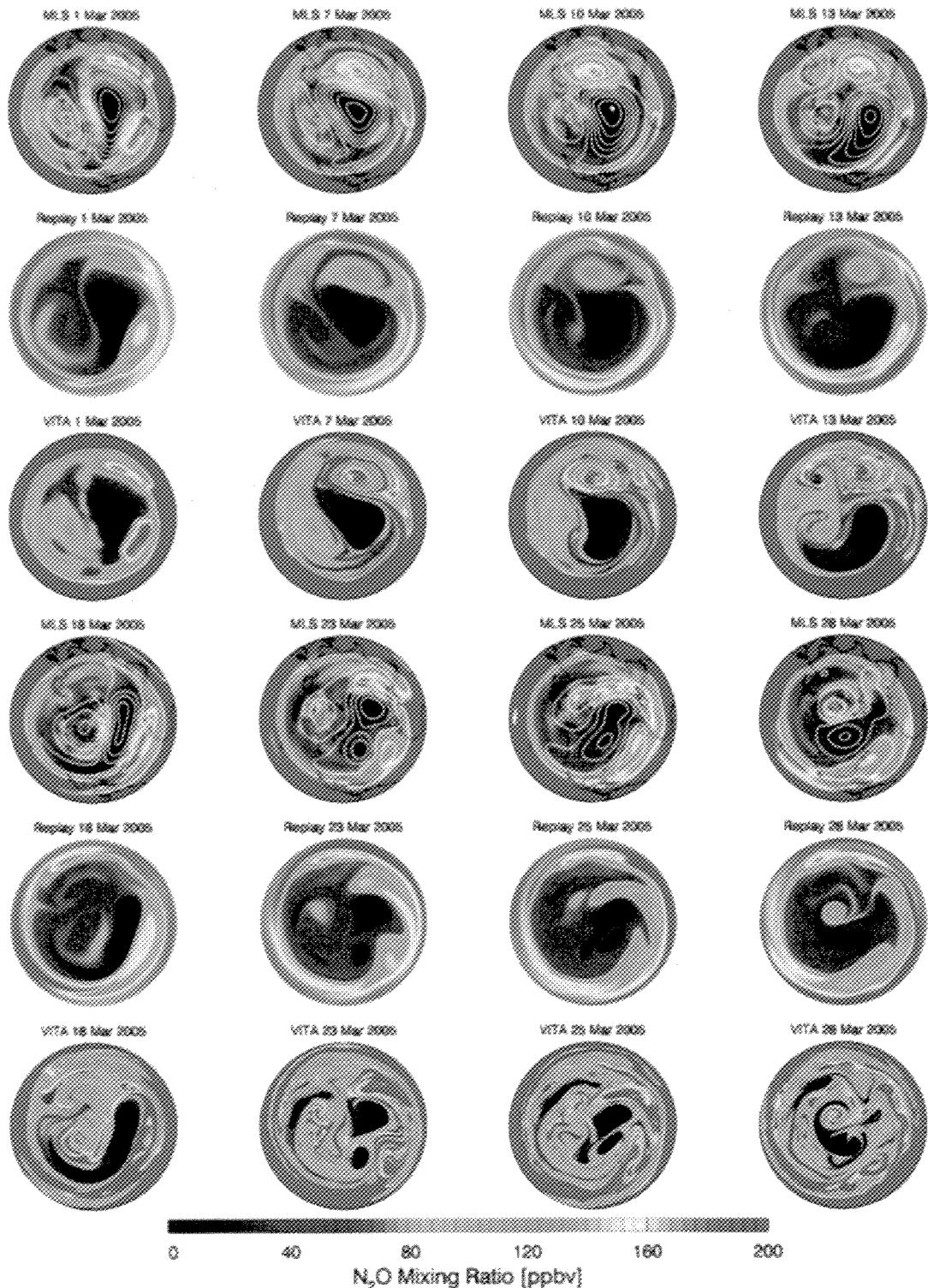
Figure 4. Northern Hemisphere EOS Aura MLS N_2O mixing ratio at 850 K for select days in March 2005 overlaid with contours of 10 hPa geopotential height at 25-m intervals (first and third rows). Replay N_2O simulations for the same days (second and fifth rows). VITA N_2O simulations initialized on 1 March 2005 (third and sixth rows).

VITA 28 Mar 2005 850 K · Replay 28 Mar 2005 850 K

N$_2$O Mixing Ratio [ppbv]

Along-Track N$_2$O (Orbit 1) · Along-Track N$_2$O (Orbit 12)
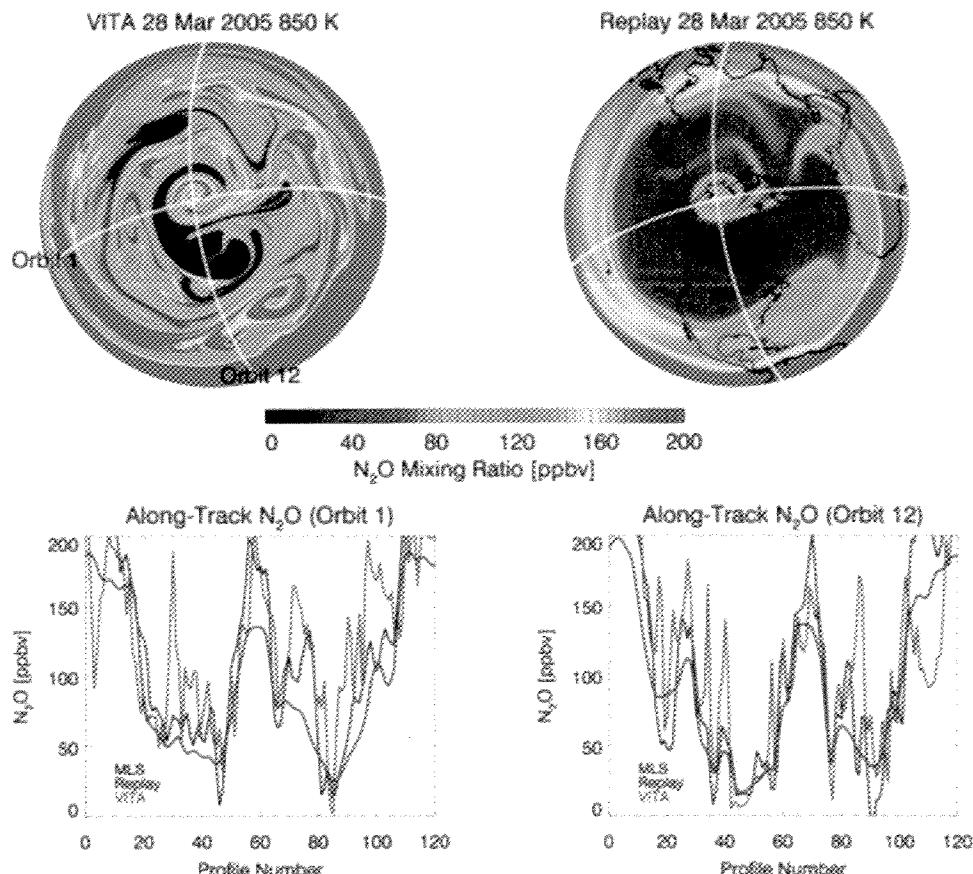
3

1
2   Figure 5.   Top row: Northern Hemisphere VITA (left) and Replay (right) N$_2$O at 850 K on 28
3   March 2005. Overlaid are two EOS Aura orbit tracks for this day. Second row: MLS, Replay,
4   and VITA N$_2$O at 850 K along the selected orbit tracks. Replay and VITA data are
5   interpolated linearly in space and time to the MLS data points.
6

MLS Along-Track N$_2$O (Orbit 1)

MLS Along-Track N$_2$O (Orbit 12)

Replay Along-Track N$_2$O (Orbit 1)

Replay Along-Track N$_2$O (Orbit 12)

N$_2$O Mixing Ratio [ppbv]
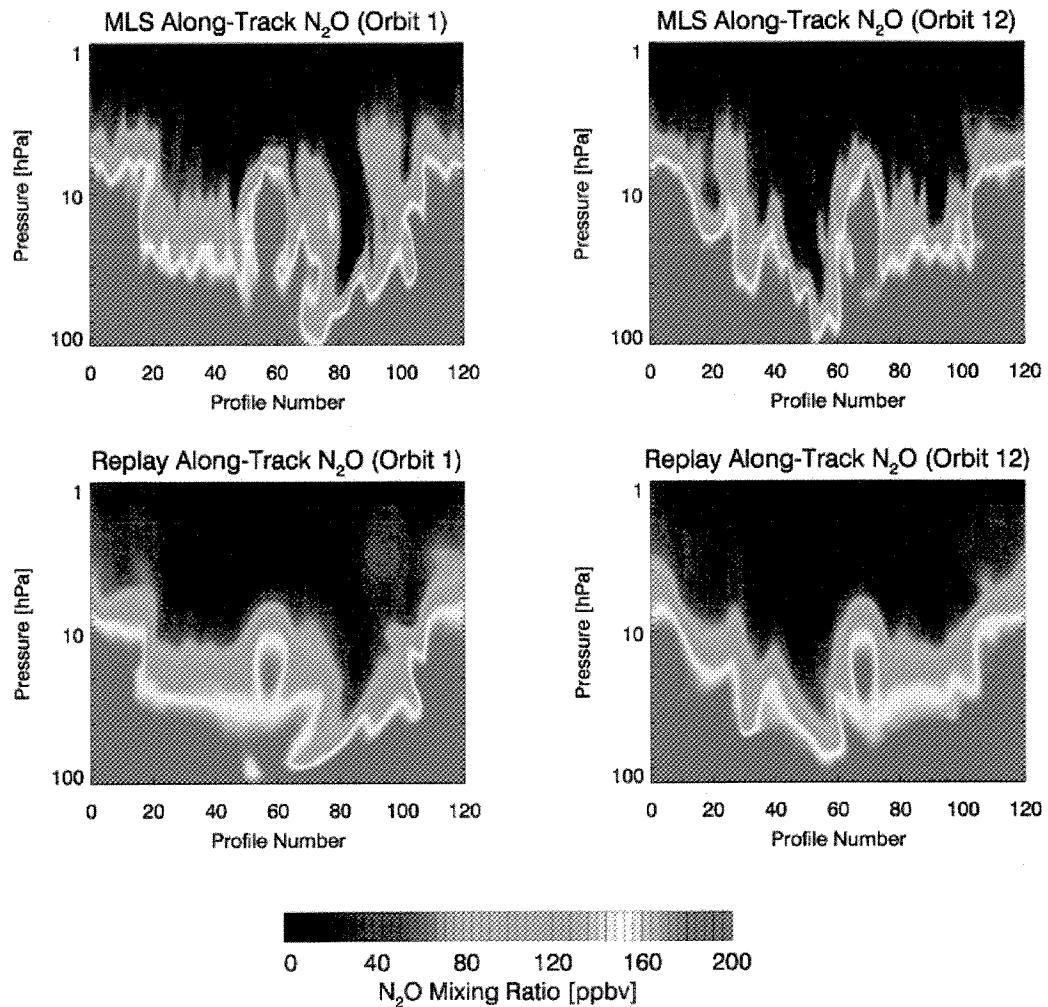
1

2   Figure 6.   MLS and Replay curtain plots (along-track cross-section as function of pressure

3   and profile number) for the two orbits shown on Figure 5.

4

5
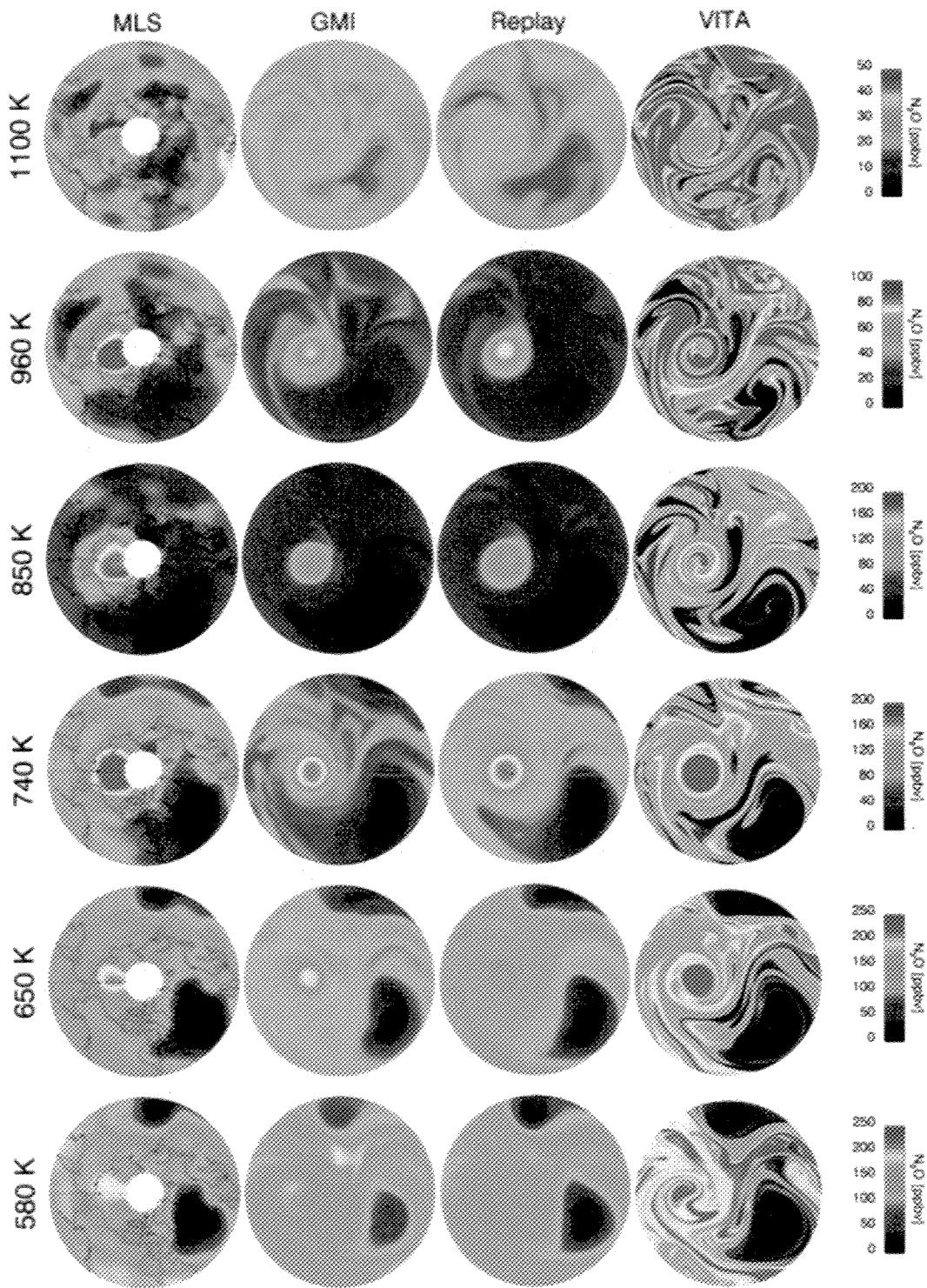
1

2　　Figure 7. MLS N_2O from 50–90°N at multiple potential temperature levels for 4 April 2005

3　　along with simulations from GMI, Replay, and VITA (see text for details).
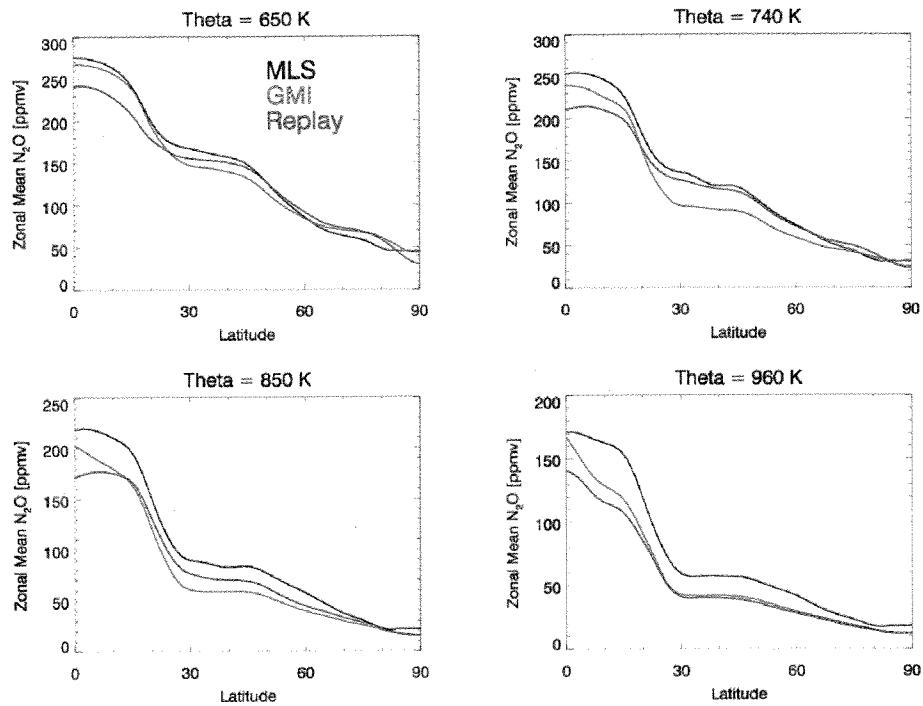
1

2   Figure 8. Zonal mean N$_2$O mixing ratios averaged from 1-10 March 2005 calculated from

3   MLS observations and GMI and Replay simulations.

4
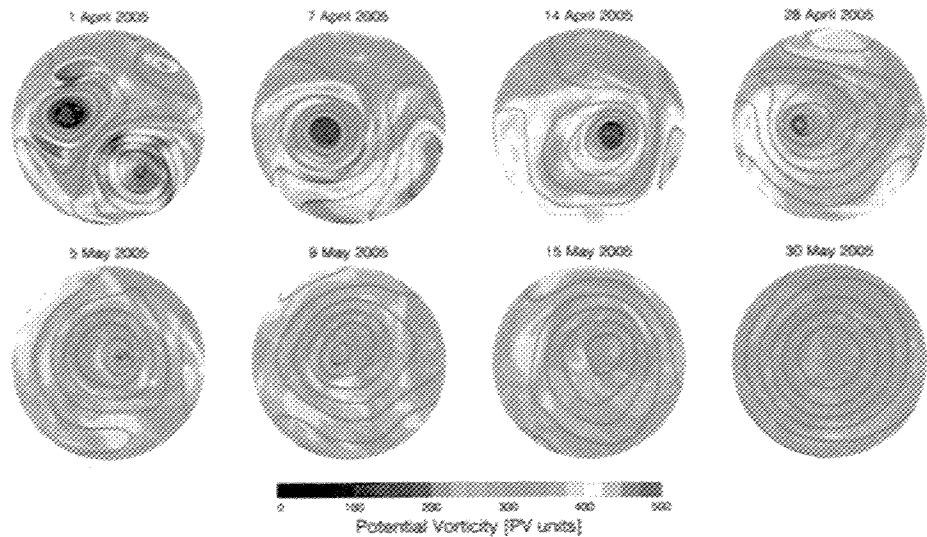
1

2   Figure 9. Ertel potential vorticity at 850 K potential temperature from 50–90°N for select days

3   in April and May 2005 (colored contours). Black lines indicate 10 hPa geopotential height at

4   10-m contour intervals.

5

6
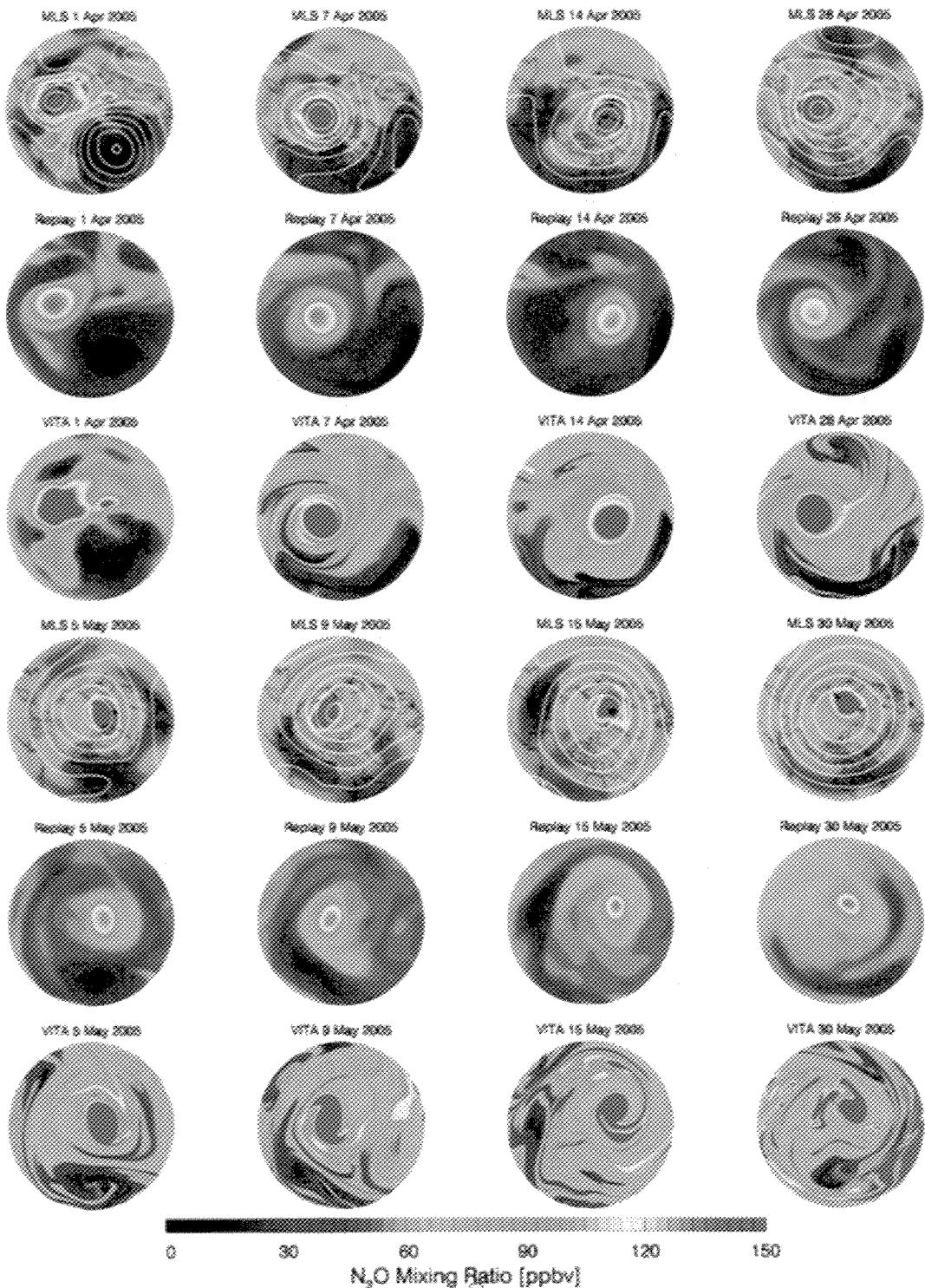
Figure 10. MLS N$_2$O mixing ratio at 850 K from 50–90°N for select days in April–May 2005 overlaid with contours of 10 hPa geopotential height at 10-m intervals (first and fourth rows). Replay N$_2$O simulations for the same days (second and fifth rows). VITA N$_2$O simulations initialized on 1 April 2005 (third and sixth rows).
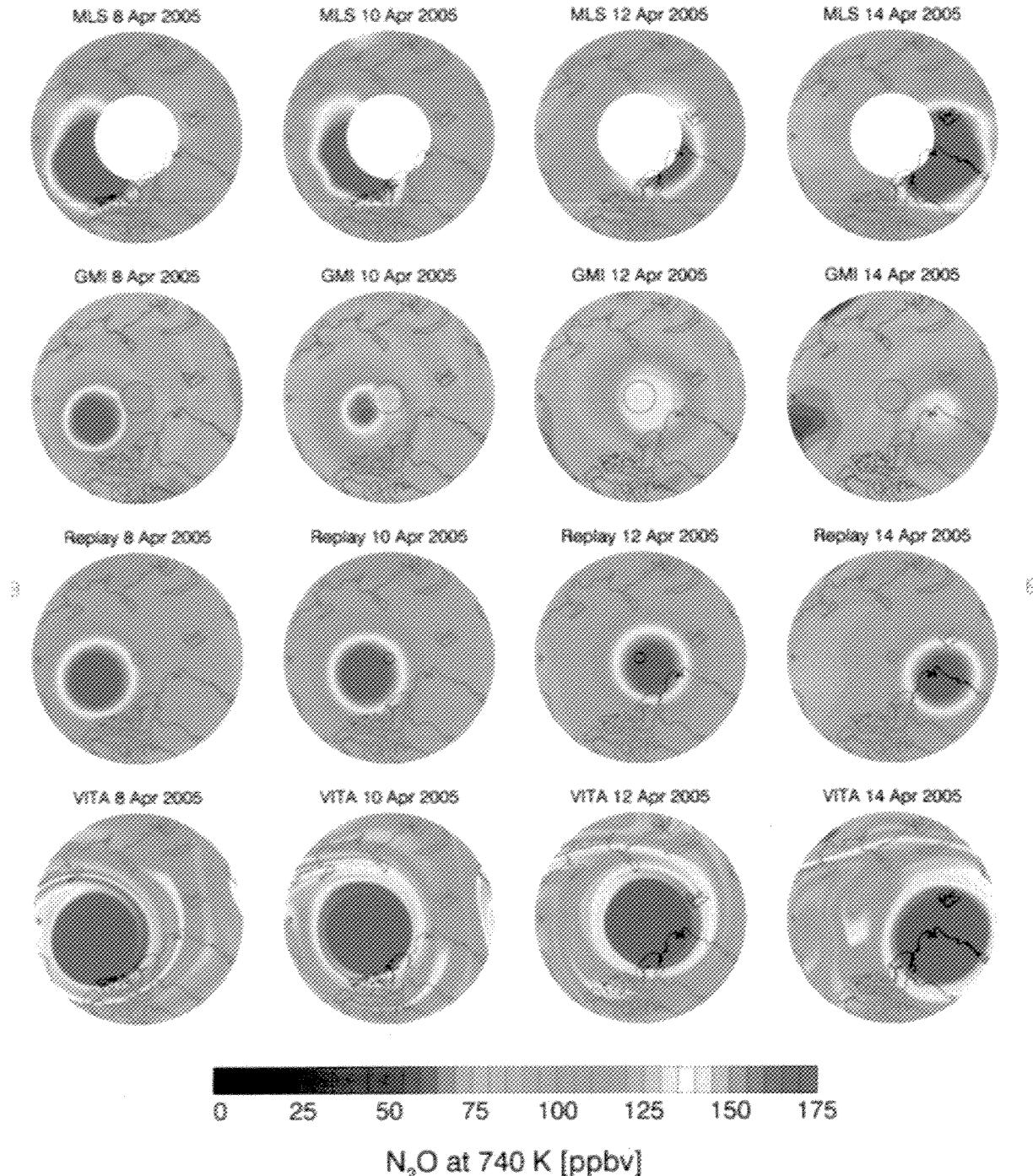
Figure 11. MLS N$_2$O mixing ratio from 70–90°N at 740 K potential temperature for 8, 10, 12, and 14 April 2005 along with simulations from GMI, Replay, and VITA. Black circles indicate the extent of the polar mixing cap in the GMI and Replay simulations.
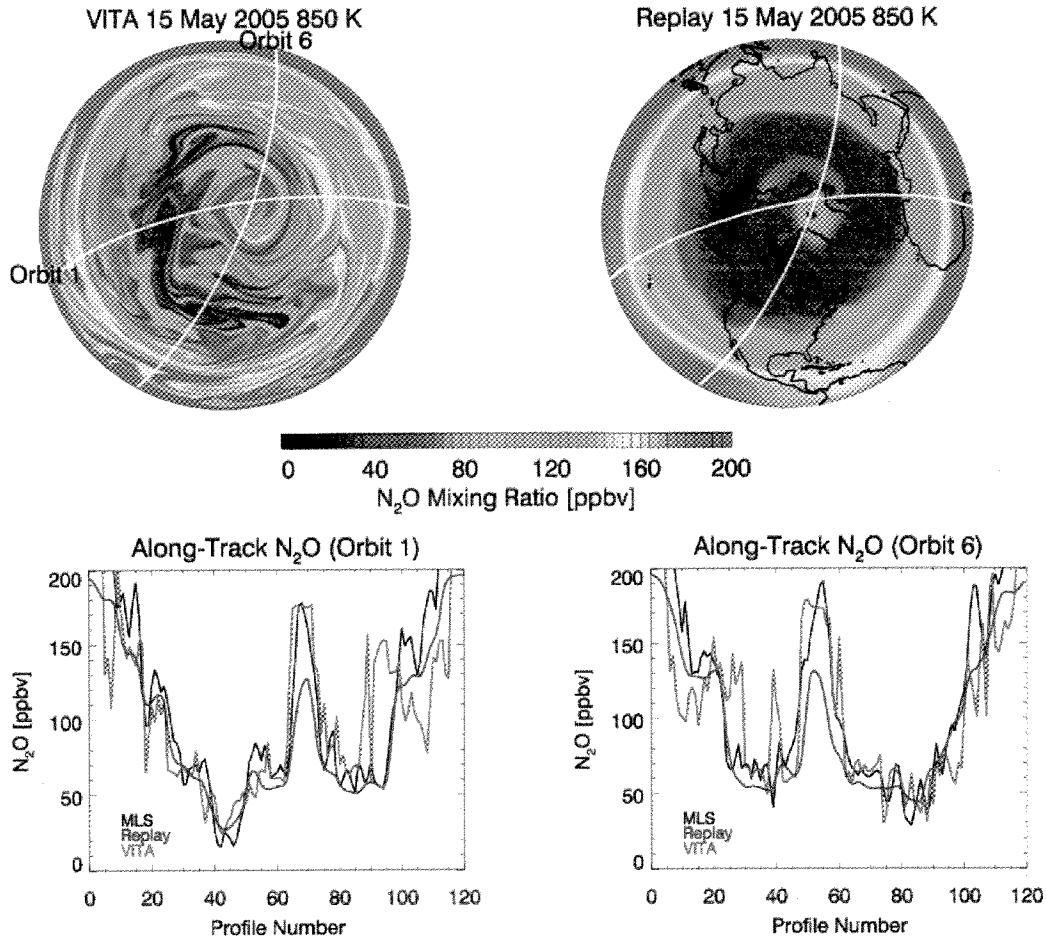
1

2 Figure 12. Top row: Northern Hemisphere VITA (left) and Replay (right) N₂O at 850 K on

3 15 May 2005. Overlaid are two EOS Aura orbit tracks for this day. Second row: MLS,

4 Replay, and VITA N₂O at 850 K along the selected orbit tracks. Replay and VITA data are

5 interpolated linearly in space and time to the MLS data points.

6
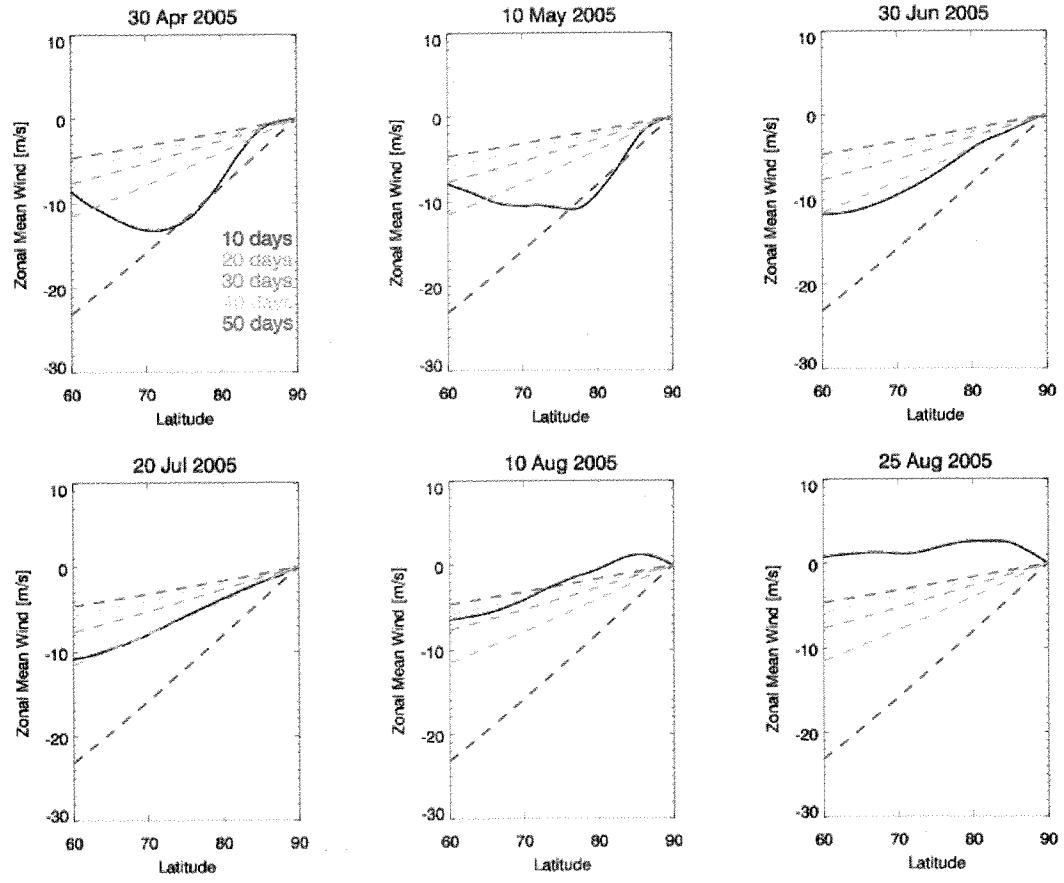
Figure 13. Zonal mean zonal wind as a function of latitude at 850 K for 30 April, 10 May, 30 June, 20 July, 10 August, and 25 August. Color curves indicate the winds necessary for solid-body rotation with periods of 10, 20, 30, 40, and 50 days.
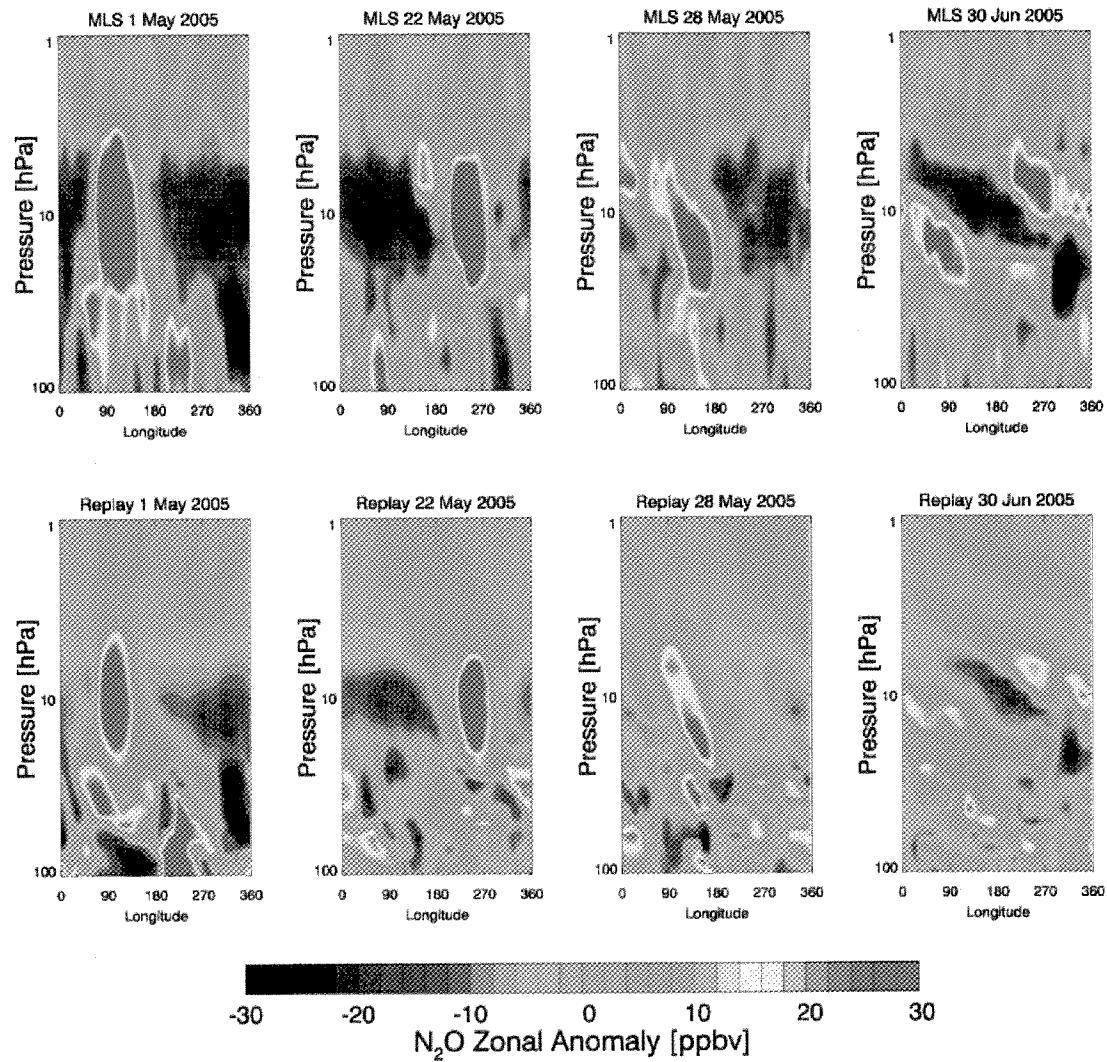
Figure 14. Longitude vs. pressure cross-sections of MLS and Replay N_2O (deviation from zonal mean) for select days in May and June 2005.

1

2   Figure 15. MLS N_2O mixing ratio at 850 K from 50–90°N for select days in June–August

3   2005 overlaid with contours of 10 hPa geopotential height at 10-m intervals (first and fourth

4   rows). Replay N_2O simulations for the same days (second and fifth rows). VITA N_2O

5   simulations initialized on 1 June 2005 (third and sixth rows).
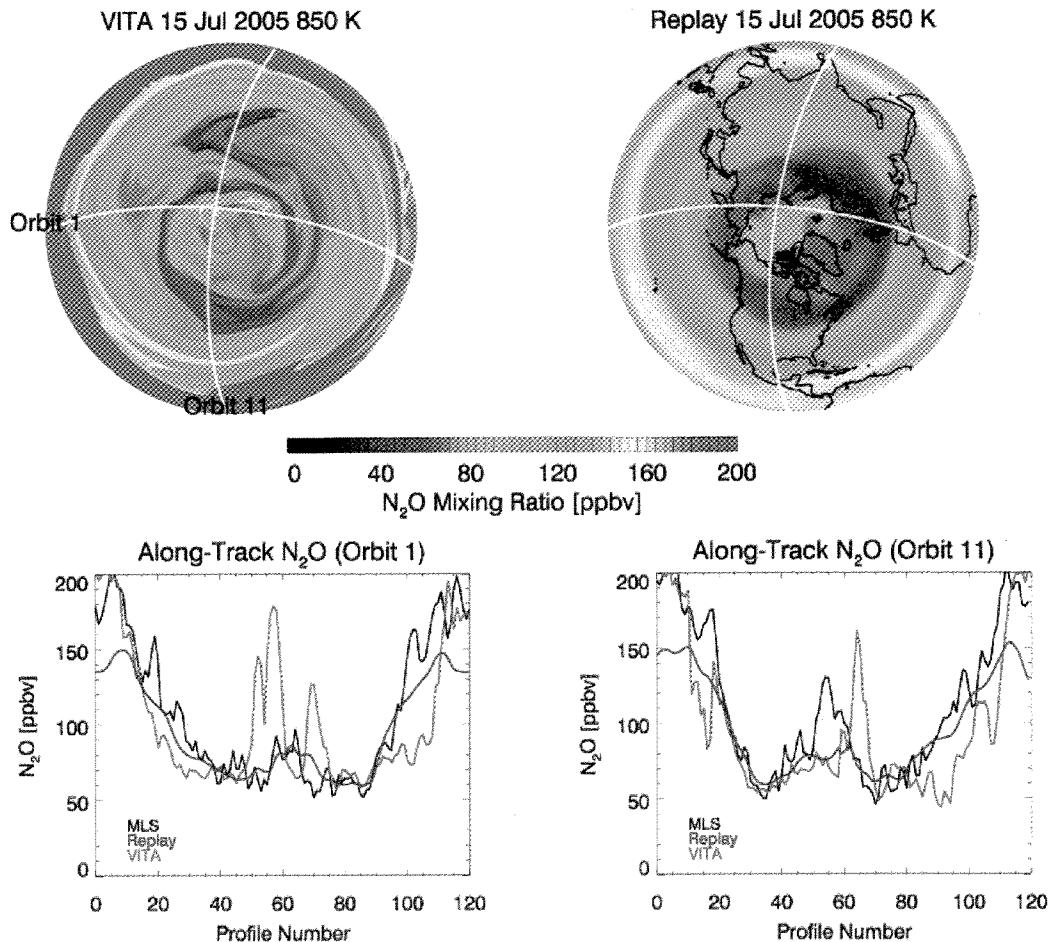
6

7   Figure 16.   Top row: Northern Hemisphere VITA (left) and Replay (right) N_2O at 850 K on

8   15 July 2005. Overlaid are two EOS Aura orbit tracks for this day. Second row: MLS, Replay,

9   and VITA N_2O at 850 K along the selected orbit tracks. Replay and VITA data are

10   interpolated linearly in space and time to the MLS data points.

11
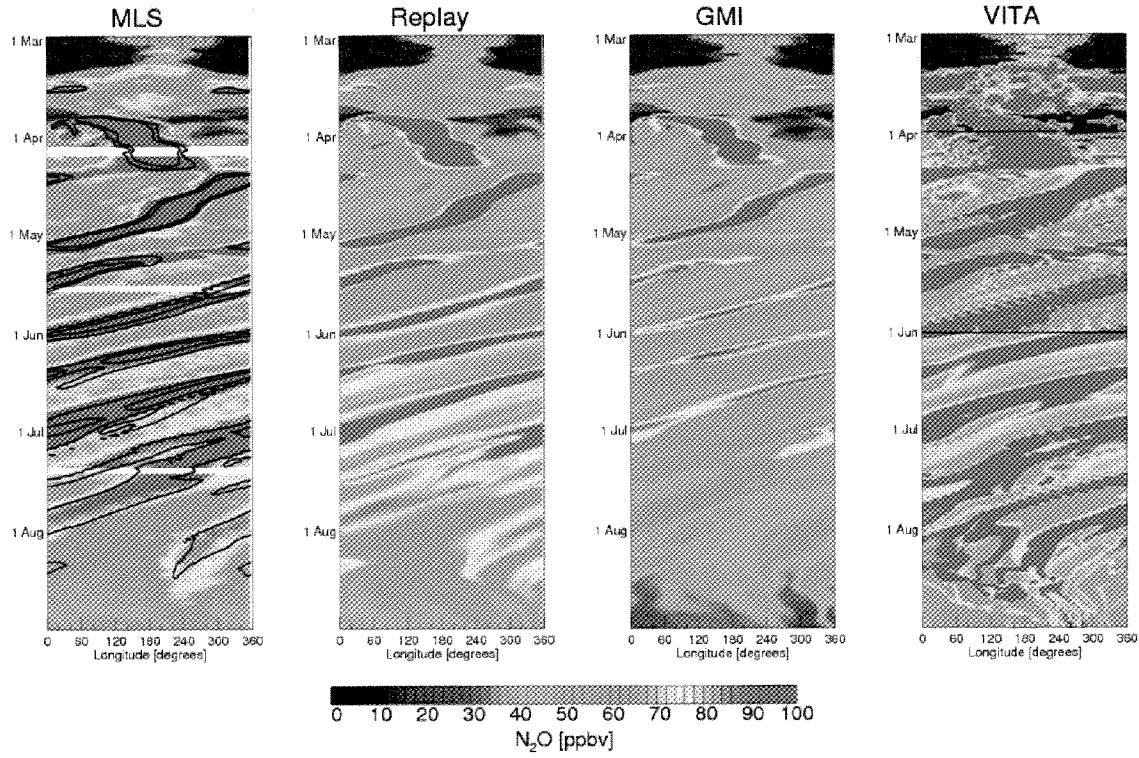
12

Figure 17. Longitude vs. time Hovmöller plots of N_2O at 850 K, 78°N for MLS, Replay, GMI, and VITA. The black contours on the MLS plot are the 75 and 100 ppbv contours of the Replay simulation, for direct comparison with MLS. White regions on the MLS plot indicate no data available during that time period. The VITA contours are produced from a composite of three runs of the model, initialized with MLS N_2O on 1 March, 1 April, and 1 June, as indicated by the horizontal black line.

Initial Tracer Anomaly

Sheared Tracer Anomaly
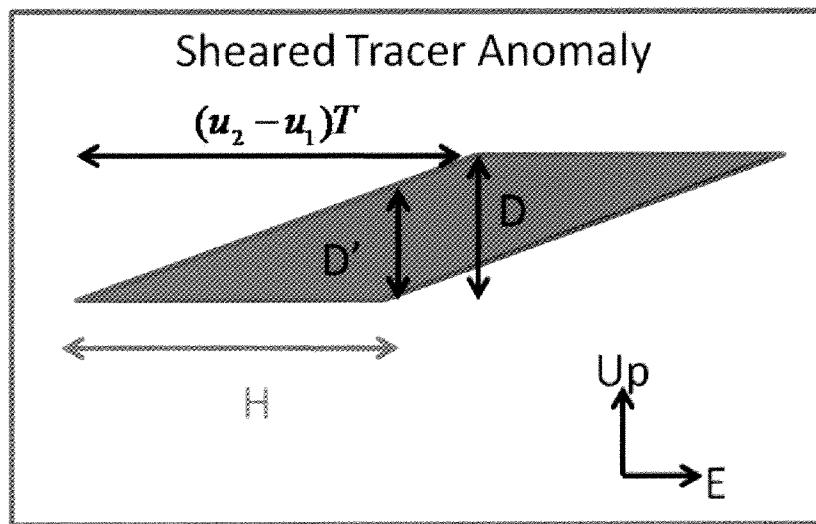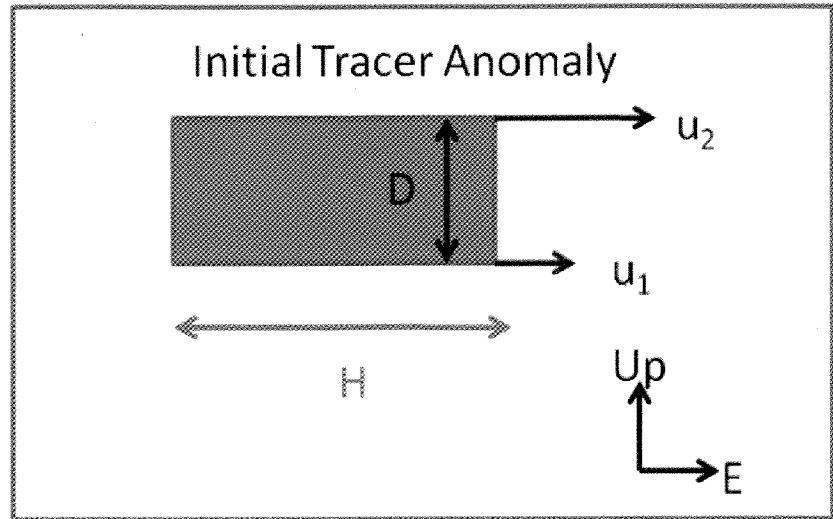
1

2   Figure 18. Schematic diagram of an idealized passive tracer anomaly subject to linear vertical

3   shear of the (steady) zonal wind. The tracer anomaly initially has a height scale D and width

4   (in the east-west direction) H. The top panel shows the initial tracer anomaly and the bottom

5   panel shows the sheared tracer anomaly at time T after the top of the anomaly has completely

6   passed the base of the anomaly. The vertical thickness of the anomaly is now D'.

7

8